Adapted ECC ozone sonde for long-duration flights aboard boundary-layer pressurized balloons

François Gheusi[1], Pierre Durand[1], Nicolas Verdier[2], François Dulac[3], Jean-Luc Attié[1,4],
Philippe Commun[5], Brice Barret[1], Claude Basdevant[6], Antoine Clenet[2], Solène Derrien[1],
Alexis Doerenbecher[4], Laaziz El Amraoui[4], Alain Fontaine[7], Emeric Hache[1,4], Corinne Jambert[1],
Elodie Jaumouillé[2,4], Yves Meyerfeld[1], Laurent Roblou[1], and Flore Tocquer[1]

[1]Laboratoire d'Aérologie, University of Toulouse, CNRS, UPS, France
[2]Centre National d'Études Spatiales, Toulouse, France
[3]Laboratoire des Sciences du Climat et de l'Environnement, IPSL-LSCE, CEA/CNRS/UVSQ, Gif-sur-Yvette, France
[4]CNRM-GAME, Météo-France / CNRS UMR 3589, Toulouse, France
[5]ALTEN, Toulouse, France
[6]Laboratoire de Météorologie Dynamique, University Pierre et Marie Curie / Ecole Poytechnique / Ecole Normale Supérieure de Paris / CNRS, Paris, France
[7]Observatoire Midi-Pyrénées, University of Toulouse / CNRS, France

Correspondence to: François Gheusi (francois.gheusi@aero.obs-mip.fr)

Abstract.

Since the 1970s, the French space agency CNES has developed boundary-layer pressurized balloons (BLPBs) with the capability to transport lightweight scientific payloads at isopycnic level and offer a quasi-Lagrangian sampling of the lower atmosphere over very long distances and durations (up to several weeks).

5   Electrochemical concentration cell (ECC) ozonesondes are widely used under small sounding balloons. However, their autonomy is limited to few hours owing to power consumption and electrolyte evaporation. An adaptation of the ECC sonde has been developed specifically for long-duration BLPB flights.

Compared to conventional ECC sondes, the main feature is the possibility of programming periodic measurement sequences (with possible remote control during the flight). To increase the ozonesonde autonomy, the strategy has been adopted of short

10   measurement sequences (2-3 min) regularly spaced in time (*e.g.,* every 15 min). The rest of the time, the sonde pump is turned off.

Results of preliminary ground-based tests are first presented. In particular, the sonde was able to provide correct ozone concentrations against a reference UV-absorption ozone analyzer for 4 days on a 15-min time base.

Then we illustrate results from 16 BLBP flights launched over the western Mediterranean during three summer field cam-

15   paigns of the ChArMEx project (http://charmex.lsce.ipsl.fr): TRAQA in 2012 and ADRIMED and SAFMED in 2013. BLPB drifting altitudes were in the range 0.25-3.2 km. The longest flight lasted more than 32 hours and covered more than 1000 km. Satisfactory data were obtained when compared to independent ozone measurements close in space and time. The quasi-Lagrangian measurements allowed a first look at ozone diurnal evolution in the marine boundary layer as well as in the lower

free troposphere. During some flight segments, there was indication of photochemical ozone production in the marine boundary layer or even in the free troposphere, at rates ranging from 1 to 2 ppbv h^{-1}.

1 Introduction

The Chemistry-Aerosol Mediterranean Experiment (ChArMEx; http://charmex.lsce.ipsl.fr) project aims at an updated assess-
5 ment of the Mediterranean atmospheric environment. The Mediterranean troposphere is indeed particularly rich in aerosol and ozone, especially during the long Mediterranean dry summer season when concentrations are higher over the basin than over most continental Europe (*e.g.,* Cuesta et al., 2013; Nabat et al., 2013). In this context, experimental campaigns including airborne observations were performed in summer 2012 and 2013 in order to document the export of continental air masses over the basin and their chemical evolution. The present article focuses more specifically on the set-up of, and first results from,
10 drifting balloons carrying ozone sondes that were deployed during those campaigns to perform Lagrangian observations of the low troposphere ozone concentration over the basin, following the former experience of Bénech et al. (2008) with shorter duration balloons.

The Lagrangian approach in fluid mechanics considers variables in a frame of reference that moves with the fluid. This is a natural point of view to deal with gas phase chemistry in the atmosphere (Businger et al., 1996, 2006). A Lagrangian
15 volume – thereafter a *parcel* – is a volume of air sufficiently small to be coherently transported by the local wind and be considered (in first order approximation) as isolated from its environment (that is, no or reduced mass exchange occurs through its boundaries). Thus, a Lagrangian air parcel can be viewed as a "smog chamber without walls" (Businger et al., 1996).

A constant-volume balloon (thereafter CVB) is generally made of a rigid pressurized envelope inflated with a mixture of helium and air, so that the lift balances the balloon weight at a given air density level. A CVB is thus drifting at nearly zero
20 horizontal velocity relative to ambient air. Under well chosen conditions with negligible vertical air motion across density levels, constant volume balloons offer a mean to perform quasi-Lagrangian measurements in the atmosphere. CVBs have been used as Lagrangian tracers as early as in the 1950s. A first use of Lagrangian balloons for comparison of turbulence with Eulerian tower-based observations was reported by Gifford (1955). Businger et al. (1996) and Businger et al. (2006) reviewed the use of CVB in atmospheric research since that early time, and also discussed their limitations as Lagrangian markers. We
25 only recall here briefly different types of use.

CVBs have been intensively used as simple trajectory markers to document air flows. For instance, positions from five balloons released together at the same density level can be used to derive the full kinematics of the flow: divergence, vorticity, and shear and stretching deformations (Businger et al., 2006). During the AUTAN 84 field campaign, CVB trajectories were used to build an interpolated wind field, the horizontal divergence and vorticity of which were derived and analyzed in relation
30 with orographic forcing (Bénech et al., 1987; Durand et al., 1993). CVB trajectories launched during the PYREX campaign (held in 1990) evidenced trapped lee waves downwind of the Pyrenees (Caccia et al., 1997). CVB trajectories were simulated in a mesoscale model through the implementation of an equation describing the balloon response to the vertical wind. This

allowed a direct assessment of the model performance comparing the simulated and observed CVB trajectories, thus coping with the non-Lagrangian character of the balloon along the vertical (Koffi et al., 2000).

With the view to measure the chemical evolution of a Lagrangian air parcel, two stategies are possible: (i) use a CVB as a Lagrangian marker, and thus as a target for a research aircraft operating measurements close to the balloon at repeated instants;
5   (ii) use directly the CVB as conveyor for onboard sensors.

The first strategy was used for instance in several Lagrangian experiments during the ASTEX/MAGE (1992) ACE-1 (1995), ACE-2 (1997) and ICARTT (2004) airborne campaigns, enabling the calculation of chemical budgets and aerosol studies in the marine boundary layer (Businger et al., 1996, 2006, and references therein).

The second strategy (onboard sensors) might be difficult to carry out for atmospheric gaseous chemistry and aerosol studies,
10   because sensors with sufficient accuracies (*e.g.,* those used aboard research aicraft) are generally too heavy to be transported by small balloons or are too expensive to be lost. Only few types of lightweight and reasonably inexpensive sensors exist, that are suitable for balloon borne measurements.

Apart from water vapour, ozone is probably the gas which is most frequently observed with balloons. It is measured worldwide on a regular time basis since the 1970s with small sounding balloons and electrochemical sensors, *e.g.,* in the frame of
15   the GAW, SHADOZ and NDACC networks (Staehelin, 2008; GAW ASOPOS panel, 2011). A more experimental alternative was a light UV-absorption sensor specifically designed for balloon flights, that was carried out during ICARTT aboard CVB (Businger et al., 2006; Mao et al., 2006).

The most frequently used ozone sensors for balloon flights are based on the principle of fast reaction of ozone with iodide ions within an electrochemical cell. Three types of electrochemical ozonesondes exist: the electrochemical concentration cell
20   (ECC), the carbon iodine cell, and the Brewer-Mast sonde (GAW ASOPOS panel, 2011, and references therein). In this study, we focus on the ECC type, which is in use in about 80% of the stations of the world wide WMO/GAW ozone sounding network. The total weight of the flight package is about 1 kg. Therefore, ECC ozonesondes are suitable for tropospheric flights aboard small CVBs. The lifetime of standard ECC sondes is however limited by power consumption but also by electrolyte evaporation. For a pump flow rate of 200 ml min^{-1} (usual value), Komhyr (1969) indicated a loss rate of about 0.2 ml per hour
25   (at 25°C, 50% humidity and sea level pressure). At this rate, the 3 ml cathode chamber of an ECC sonde would be emptied within 15 h, but in reality, the sonde performance lowers well before this time because the ozone measurement is to some extent sensitive to the electrolyte concentration (see *e.g.,* Smit et al., 2007, and also the discussion in Sect.3.2).

Bénech et al. (2008) carried out standard ECC ozonesondes aboard CVB for up to 6-hour flights in the boundary layer and the lower free troposphere during two ESCOMPTE field campaigns in 2000 and 2001, taking place on the French Mediterranean
30   coast (Cros et al., 2004)[1]. From flight segments during which the balloons remained in the same homogeneous air mass, the authors were able to quantify quasi-Lagrangian ozone growth rates due to photoproduction in the polluted summer boundary layer, ranging from zero to 13 ppbv h^{-1} around a mean value of 6 ppbv h^{-1}.

---

[1]Note that in 2000-2001, radio transponders were used for data transmission. Thus, the balloon autonomy was also limited by the range of radio transmission, despite the deployment of a regional network of radio receivers during the campaigns.

As early as in the 1970s, the French space agency CNES (Centre National d'Études Spatiales) developed constant volume balloons for long-range scientific flights in the boundary layer or the low troposphere, called *boundary-layer pressurized balloons* – thereafter BLPBs (Cadet et al., 1975, 1981; Ethé et al., 2002, – more detail on the recent generation of BLPB is given below in this article). The use of satellite data transmission allows for flights over several days or even weeks. Clearly, standard ECC ozonesondes are not suited for such long-duration flights. Concerning power consumption, the ozonesonde lifetime can be considerably increased by use of high performance lithium batteries. In spite of this, the issue of electrolyte evaporation remains. An ECC ozonesonde in continuous working would not be able to cover a complete ozone diurnal cycle.

For this reason, we present in this article a specific adaptation of ECC ozonesondes, whereby the sonde alternates between short working periods and longer rest periods in order to save electrolyte and increase the sonde lifetime up to several days. All technical details are given in Section 2. Laboratory tests presented in Section 3 were preliminary to flights aboard BLPB during three fields campaigns in the western Mediterranean during summer 2012 and 2013, that are detailed in Section 4. The main results are summarized in the concluding Section 5.

2 ECC ozonesonde and specific adaptations

In all our experiments, we used commercial En-Sci "Z" ECC ozonesondes[2], either in their original form for conventional balloon soundings, or in a specific implementation for flights aboard CNES constant-volume balloons. In the latter case, only few elements of commercial En-Sci Z sondes were kept (Sect.2.2.2).

2.1 ECC ozonesonde general features

Electrochemical concentration cell (ECC) ozonesondes developed by Komhyr (1969) are among the most commonly used worldwide for tropospheric and stratospheric ozone soundings (Smit et al., 2007; GAW ASOPOS panel, 2011). Ozone mole fractions $x_{O_3} = P_{O_3}/P$ (P being ambient pressure and P_{O_3} ozone partial pressure) can be obtained from the sonde data as:

$$x_{O_3} = \frac{R}{2F} \frac{T}{P} \frac{I - I_0}{Q_v}, \tag{1}$$

where $R = 8.31$ J mol^{-1} K^{-1} is the universal gas constant, $F = 96485$ C mol^{-1} is the Faraday constant, T is the pump temperature, I is the current measured in the ozonesonde, I_0 is the sonde background current (residual current in absence of ozone) and Q_v is the pump volumic flow rate. T, I and P are directly measured on board during the flight, while I_0 and Q_v are derived from pre-flight laboratory measurements. Eq.1 derivation as well as details on the introduced variables and data processing are given in Appendix A.

For all experiments, we used electrolytic solutions recommended for ozonesonde measurements by the GAW panel of experts (GAW ASOPOS panel, 2011) after consideration of several ozonesonde intercomparison experiments (Smit et al., 2007; Deshler et al., 2008). For En-Sci ECC sondes, the recommended cathode solution is the "0.5% half-buffer" (as termed in Smit et al., 2007). The anode and cathode solution compositions are given in Appendix B1. For all flights, we charged the

---

[2]Now manufactured by Droplet Measurements Technologies, Colorado, USA.

ECC sonde chambers with 3 ml of cathode solution and 1,5 ml of anode solution. All other details on sonde preparation and control are given in Appendix B2.

GAW ASOPOS panel (2011) indicate that standard ECC ozonesondes operated carefully have a precision below 5% and an absolute accuracy below 10% in the troposphere. They also review in great detail the contributions from each instrumental

5 variables in Eq.1 to the overall uncertainty (their Figure 3-1). In the troposphere, it is clearly dominated by the contribution of the uncertainty on the background current I_0. The uncertainties on the other variables contribute together by less than 1% of the ozone mole fraction value.

2.2 Specific implementation aboard CNES boundary-layer pressurized balloons

2.2.1 BLPB overview

10 The CNES BLPB consists of a spherical, non-dilatable and pressurized envelope filled with a mixture of helium and air (Ethé et al., 2002, and Fig.1). As the balloon volume and mass are constant, the BLPB flies at constant-density (isopycnic) levels in the atmosphere. The desired flight level can be adjusted through the total mass of the balloon, by varying the quantity of gas in the balloon (related to internal pressure) or the proportions of air and helium. Two possible diameters exist: 2.5 m and 2.6 m. The bigger version is used to reach higher altitudes (2000-3300 m above the launch base).

15 The data exchange between the balloon and the operation centre is enabled from anywhere on Earth through Iridium satellite phone connection. This allows for long-range flights (possibly several weeks). In absence of navigation constraint, the only limitation is the battery autonomy. However, during the 2012 and 2013 campaigns over the western Mediterranean, flights were restricted for security reasons to a delimited zone over sea and over a number of islands for short transits (Fig.2). The flights automatically aborted when the balloons exited from the authorized flight zone (or were aborted upon request from the

20 operation centre). To abort the flight, a heated wire device perforates the envelope. The balloon slowly loses its gas and softly touches down after a few minutes.

There are three different payloads aboard a BLPB, which are located either at the "north" (upper) or "south" (lower) pole of the balloon (Fig.1):

– the housekeeping gondola (south-pole, inside the envelope) is devoted to navigation control, communication with the
25 other payloads, and remote data transmission and control (plus a redundant GPS).

– the north-pole science gondola (outside the envelope) includes the main GPS, and weather sensors of ambient temperature, pressure, humidity and global radiation.

– the south-pole scientific payload (outside the envelope) is devoted to specific sensors. During the 2012 and 2013 campaigns, this payload was either the ozone sensor under consideration in this article, or the LOAC[3] sensor for measurement
30 of aerosol properties (not in the scope of the present article, see Legain et al., 2013; Renard et al., 2015a, b).

---

[3]*Light Optical Aerosol Counter.*

It is seen here that the south-pole ozone sensor is located close to the balloon envelope (air inlet approximately 20 cm below) and the question arises whether ozone deposition on the envelope could perturb measurements. To answer this question, a test was conducted where the air inlet of a UV ozone analyzer was equipped with a sampling head made of the balloon envelope material (an inextensible polymer). The sampling head consisted of a thin cone (length of about 25 cm and maximum diameter

5 of 2-3 cm) through which ambient air flowed before entering the teflon air inlet of the analyzer. No detectable change in the analyzer ozone reading was observed with or without this sampling head. No significant perturbation is thus to be expected due to the balloon proximity.

2.2.2 Ozone payload

In the specific implementation of ECC ozonesonde for BLPB, the motor, the pump, the electrochemical cell and the teflon

10 tubing of original En-Sci Z sondes were disassembled then remounted on an entirely new electronic card (Fig.3). Compared to the standard electronic implementation of ECC sondes, the major specific features are the following:

– In standard sondes, the electronic card and the pump motor are powered by separate batteries (9 V and 12 V, respectively). In the BLPB implementation, both motor and electronics are powered by a single lithium 3.6 V battery ($Li-SOCl_2$). The motor voltage is electronically multiplied up to about 10 V. Its rotation speed is a bit lower than under nominal

15 voltage (12V), but this affects the pump flow rate by only few percents.

– The motor is switched on or off by electronic command following a programmable sequence described below.

The measurement sequence (Fig.4) is characterized by three different time intervals, namely T_0, T_1 and T_2, which are the overall period of the sequence, the duration of a spin-up phase, and the duration of the measurement phase, respectively. More precisely,

20 – the sonde motor is switched on at $t = nT_0$ (where n is an integer).

– from $t_0 = nT_0$ to $t_1 = nT_0 + T_1$ (spin-up phase), the current in the electrochemical cell is establishing. Two current values are recorded during this interval to check how fast the current reaches its asymptotic value (Fig.4, cyan points).

– from $t_1 = nT_0 + T_1$ to $t_2 = nT_0 + T_1 + T_2$ (measurement phase), current intensities are regularly recorded (Fig.4, blue points).

25 – the sonde motor is switched off from $t_2 = nT_0 + T_1 + T_2$ to $t = (n+1)T_0$ (rest phase).

Note that T_0 must be greater than $T_1 + T_2$. The values mostly used during the 2012 and 2013 flights were $T_0 = 900$ s (15 min), $T_1 = 60$ s and $T_2 = 120$ s. This choice was inferred from laboratory tests presented in Sect.3.

The sonde can also work in continuous mode as in a classical sounding. This is interesting during the BLPB ascent phase to profile the lower atmosphere. In this case, the user simply has to set $T_0 = 0$ (whatever T_1 and T_2). In this mode, current

30 intensity data are recorded every 10 s. The continuous mode was used for the 2013 campaigns during the launch and ascent

phases (Sect.4.2.1). Once the balloons had reached their ceiling altitude, cruise values for the T_i were sent by remote control from the operation centre.

3 Laboratory tests

3.1 First tests in intermittent mode

3.1.1 Ozone current establishment

A first experiment was conducted on 12 May 2011 at a fixed outdoor place to investigate the behaviour of an ECC ozonesonde (the experimental sonde, hereafter referred to as S_{Exp}) alternating rest (sonde motor off) and run (sonde motor on) phases, and to evaluate its ability to reproduce correct ozone mole fractions against reference measurements. The latter were (i) a standard (En-Sci Z) ECC ozonesonde working as usual in continuous mode (the reference sonde, hereafter S_{Ref}); (ii) a UV-absorption analyzer (TEI 42i). The expected absolute accuracy is below 10% for the reference sonde in the troposphere (GAW ASOPOS panel, 2011), while it is better than 3 ppbv for the UV analyzer. The latter value was obtained combining (as rooted sum of squares) the uncertainties given in Gheusi et al. (2011) for the analyzer measurement itself (1.2 ppbv) and the calibration chain (2.3 ppbv).

The time series of ozone mole fractions from the experimental sonde, the reference sonde and the UV analyzer are summarized in Fig.5. The alternation of run and rest phases is well visible for S_{Exp} with various run/rest sequences of 10min/10min, 5min/5min and 3min/3min. It is also seen that every time the motor restarts, the ozone current (mole fraction) in S_{Exp} rapidly grows from almost zero to values comparable to the references (Fig.4 and 5).

The current establishment is investigated more quantitatively from the data presented in Fig.6. In a first step, we compared to the reference sonde the S_{Exp} values taken at least 180 s after switch-on, when the ozone current is well established (Fig.6a). A fair agreement is found ($r^2 = 0.79$; bias $b = \overline{x_{Exp}} - \overline{x_{Ref}} = 0.9$ ppbv; bias-corrected standard deviation: $\overline{(x_{Exp} - x_{Ref} - b)^2}^{1/2} = 0.7$ ppbv). Note that the bias corresponds to a current offset of about 0.025 μA, which is typically the range of uncertainty on the background current (GAW ASOPOS panel, 2011).

The linear model provides the predicted ozone value for S_{Exp} for a given value of S_{Ref}. In a second step, real data from S_{Exp} are compared to the prediction, as function of time elapsed since last S_{Exp} motor restart (Fig.6b). It is seen that after a rapid growth phase, a $\pm 10\%$ agreement is achieved within a few tens of seconds. This is an expected result since ECC ozone sensors are known to have response time to a step change in ozone of 20-30 s (GAW ASOPOS panel, 2011). In the following, we therefore adopt a spin-up time $T_1 = 60$ s after every motor restart before considering measurements as valid.

3.1.2 Pump flow in spin-up regime

Pump flow rates are generally measured once for all at ground level during the pre-flight preparation, then a pressure-dependent correction factor is applied during the flight (see Appendix A2.2). The flow rate measurement is usually performed with the motor having been running for a few tens of minutes (see Appendix B2.2).

BLPB ozonesondes are designed to work for a few minutes between longer periods of rest. We investigated by a laboratory experiment whether after some period of rest, the pump flow rate of an En-Sci Z ECC sonde varies in the first minutes after restart. To this goal, we made measurements with a soap-film flowmeter, but in a timed way with respect to the instant of motor start.

5   More specifically, the sonde motor and a stopwatch are simultaneously started at $t = 0$. A soap film is generated after a few seconds. The time t_0 when the film passes at 0 ml is recorded, as well as the time t_1 when it passes at 100 ml. The stopwatch still running, a second film is generated, and times t_2 at 0 ml and t_3 at 100 ml are recorded – and so on with n successive films. As a result, t_{2i} and t_{2i+1} $(i = 0, .., n)$ are respectively the beginning and end times of the ith measurement interval (ith soap film), and $Q_{vi} = V_0/(t_{2i+1} - t_{2i})$ is the corresponding pump flow rate ($V_0 = 100$ ml, see App.A). As the latter value represents

10   a mean flow rate over this time interval, we finally consider the middle time $(t_{2i} + t_{2i+1})/2$ as the measurement time for Q_{vi}.

We present here the results of seven measurement sequences conducted as described above with the same sonde motor and pump. Between each sequence, the motor was let at rest for at least 5 minutes. The obtained flow rates range between 0.206 and 0.212 l min^{-1}. Figure 7 shows the evolution (relative variation) of the pump flow rate during a few tens of seconds after motor start. Globally, there is a decay of the pump flow rate within the first two minutes. The decay is in the range 0-1.7%

15   between 60 s (the beginning of the measurement phase) and 120 s.

This might induce comparable variation of the ozone current in the sonde cell for a given ozone concentration in air (Eq.A1). If the ozone mole fraction is retrieved from ozone current measurement using a constant value for Q_v measured as usual during the flight preparation (Eq.1), the result might be affected in the same way (about 2%) due to unmeasured flow rate variation during the measurement phase. This is therefore a source of uncertainty that adds to those already reported in the literature

20   concerning the flow rate determination. For instance, GAW ASOPOS panel (2011) reports $\pm 1\%$ of uncertainty in the flow rate measurement by soap film displacement technique.

From Fig.7 it is difficult to characterize a variation law for the flow rate that could be reliably used as correction factor for ozone mole fraction retrievals. For a future version of the BLPB ozonesonde, it would be interesting to develop an onboard measurement of the flow rate – providing a sufficient accuracy (less than 1%) could be achieved with a light sensor.

25   We will continue in the present study to use constant flow rate values determined as usual. However, a 2% uncertainty on ozone mole fraction attached to flow rate variation during the BLPB sonde work phase should be kept in mind.

3.2   Long-duration test in realistic conditions

We present here a ground-based experiment conducted from 31 May to 6 June 2012 to test the ability of the BLPB ozonesonde to monitor the evolution of ozone in the boundary layer over several days. At this stage of development, the sonde version was

30   the same as those that flew few weeks later over the Mediterranean during the 2012 campaign (see Sect.4). This experiment was also the opportunity to test the Iridium satellite connection. A TEI 49i UV-absorption ozone analyzer was again deployed in the vicinity of the BLPB ozonesonde.

The values for the sonde measurement cycles were $T_0 = 900$ s (overal period), $T_1 = 60$ s (spin-up phase) and $T_2 = 60$ s (measurement phase). During each measurement phase, 12 values of ozone current were recorded, then converted in ozone

mole fractions using a background current $I_0 = 0.13$ μA, a pump time $t_p = 32$ s (100 ml)$^{-1}$, and the ambient pressure and pump temperature provided by the sonde at each measurement phase. The 12 mole fractions were finally aggregated in a single mean value (and corresponding standard deviation) available every 15 min.

The time series of ozone mole fraction from both instruments are shown in Fig.8(a). The BLPB ozonesonde was able to provide realistic measurements with respect to the UV analyzer (± 10 %) almost all along its lifetime, i.e. 5 days. In particular, the ozone diurnal cycles occuring during these sunny days were well captured, as well as variations on shorter time scales (*e.g.,* on 3-4 June 2012). The linear correlation between these measurements is fair (Fig.8b: $r^2 = 0.88$; bias: -3.3 ppbv; standard deviation of sonde minus analyzer: 5.6 ppbv).

The sonde lifetime was limited by cathode solution evaporation. In our experiment ($T_0 = 900$ s; $T_1 = T_2 = 60$ s), the sonde worked during 3.2 hours per day. At the evaporation rate reported by Komhyr (1969) (about 0.2 ml per work hour for a pump flow rate of 200 ml min^{-1}), the solution would have completely evaporated in 4.7 days. This is consistent with the duration of our experiment.

It is interesting to focus on the spin-up phase of each measurement cycle, and its evolution through the sonde lifetime. For each sonde measurement cycle, we compare the values measured by the sonde 20 and 40 s after motor start, with the mean of the 12 mole fractions recorded during the measurement phase (established current) between 60 and 120 s after motor start (Fig.9a). During the first day, the ozone current reaches 60% (resp. 90%) of the established value 20 s (resp. 40 s) after the motor start. This is consistent with the result presented in Fig.6(b). Over several days, both percentages are seen to grow with time. By the end of the experiment, the 20-s values are near 90% and the 40-s values above 95%. This means that the response time is shortening, or in other words, that the ozone sensor tends to be faster. This is due to progressive evaporation of the electrolyte in the cathode chamber. A current is induced in the electrochemical cell when some desequilibrium is created due to I^- oxidation by ozone, enhancing iodine concentration in the cathode solution (reaction AR1 in App.A). An excess in I_2 concentration is all the later to appear that the solution volume (and hence the total amount of ions to oxidize) is large. As a result, the ozonesonde response time is an indicator of the cathode solution level, and to some extent could be used as electrolyte gauge for long-duration flights.

Figure 9(b) also shows an evolution through the sonde lifetime of the absolute deviation from the UV analyzer reference. This deviation tends to increase with time. A linear regression indicates a growth of 1.63 ppbv day^{-1} (≈ 0.07 ppbv h^{-1}). This drift could also be linked to cathode electrolyte evaporation, which tends to increase the ion concentrations in the solution. In our experiment where the sonde ran until almost complete evaporation, the cathode concentrations might have doubled at half time, i.e. after about 2.5 days. From the JOSIE 2000 experiment, Smit et al. (2007) reported for ECC sondes 5% larger ozone values when using a cathode solution with doubled concentrations with respect to the "0.5% half-buffer" solution (used to fill the cathode chamber – App.B1).

A great number of similar long duration tests against a reference measurement would be needed to demonstrate the link with evaporation and to characterize the drift. The present result at least suggests that observed ozone trends lower than a few 0.1 ppbv h^{-1} should be considered cautiously.

4 BLPB ozonesonde flights over the Mediterranean

4.1 Operational overview

Sixteen BLBP flights equipped with an ozonesonde were launched in the low troposphere over the Mediterranean Sea during three field campaigns of the coordinated project ChArMEx (http://charmex.lsce.ipsl.fr): TRAQA[4] in summer 2012; ADRI-

5 MED[5] and SAFMED[6], in summer 2013. Each campaign had its own launch site (Fig.10 and Tab.1) selected for both scientific and practical reasons. All launch sites were located either on a coast or an island to avoid flight over inhabited areas just after launch. TRAQA and SAFMED (Di Biagio et al., 2015) were devoted to anthropogenic pollution transport and chemistry. The launch sites (Martigues and Levant island, respectively) were located on the French Mediterranean south-east coast, which is a densely inhabited and industrialized area, and therefore a major source of pollution in the western Mediterranean basin. The

10 BLPB density was tuned for low altitude flights in the marine boundary layer or the lower free troposphere (300-900 m, Tab.2). ADRIMED (Mallet et al., 2016) focused mainly on the aerosol optical properties, especially in case of dust transport from the Saharan desert in the free troposphere. Possible influence on ozone was also investigated. The chosen launch base was on the Minorca island. BLPB flights were performed at higher altitude (2000-3000 m, Tab.2).

Table 2 summarizes the overall performance achieved by the ozone BLPBs during the campaigns. Except in three cases

15 (namely B53, B62 and B69), all flights were terminated when they reached the limit of the authorized flight zone (Fig.2 and 10). B53 (from Minorca Isl.) was prematurely aborted because of remote connection failures. B62 and B69 (from Levant Isl.) were aborted owing to uncontrolled fall below a critical flight altitude (200 m, defined for safety reasons – risk of a sea surface touchdown which could damage the navigation gondola and render the balloon out of control). This occured at night for both flights and might be caused by condensation on the envelope which weighted the balloon. For all flights (incl. B53, B62 and

20 B69) excepting B61, the ozonesonde worked obviously well until the flight end. In the course of flight B61, the ozone signal was suddenly lost after a turbulence[7] area over the crests of Cape Corsica (the elongated mountain chain forming Corsica's "index finger"), but the ozonesonde gave no sign of anomaly before that time. The other payloads on B61 went on working well for hours. The BLPB flight durations and ranges are reported in Tab.2. In most cases, the BLPB ozonesondes provided data over the full flight durations, which are well beyond the lifetime of classical ozonesondes (Bénech et al., 2008, report no ozone

25 records longer than 6 h.). The ability to cover a full diurnal cycle was demonstrated on the occasion of favorable trajectories (*e.g.,* B55, B57, B62, B64, B69).

---

[4]French acronym for *TRAnsport and Air Quality*.

[5]*Aerosol Direct Radiative Impact in the MEDiterranean*.

[6]*Secondary Aerosol Formation in the MEDiterranean*.

[7]GPS-derived balloon vertical velocity showed quick variations with 30-s averaged values larger than $1~\mathrm{m~s^{-1}}$.

4.2 Inflight validations

4.2.1 BLPB ascent profiles compared to conventional ozone soundings

During the 2012 and 2013 campaigns, conventional radiosoundings including ECC ozonesondes were operated in addition to BLPB launches. Some of them were launched sufficiently close in time to BLPBs (namely, B53, B54, B61 and B69) to allow

5 for comparisons of the ascent profiles. Two other BLBPs (B64 and B65) were also launched simultaneously and compared to each other. Such profile comparisons were only possible in 2013 because before that time, the BLPB ozonesondes did not allow for continuous working mode during the launch and ascent phases.

Those radiosoundings and BLPB ascent profiles are displayed in Fig.11. Globally, balloons launched sufficiently close in time (typically one hour or less) reveal very similar ozone profiles, whatever the type of balloon (BLPB or conventional

10 sounding balloon) or ozonesonde (adapted or conventional ECC). This illustrates the correct behaviour of the adapted ECC sondes when used in continuous mode, and is also an indication that the proximity of BLPB envelope from the sonde air inlet does not significantly perturb the ozone measurements even during the balloon ascent, which is the worst configuration since the sonde is in the wake of the balloon. Note, however, that these comparisons cannot be considered as validation elements for the intermittent working mode used during the BLPB cruise at ceiling levels.

15 4.2.2 BLPBs at ceiling

Once the BLPBs have reached their ceiling level, it was uneasy to carry out ozone measurements specifically to validate the BLPB ozone data. We nevertheless tried to compare these data to other coexisting ozone data whenever possible.

During TRAQA, it was attempted to arrange in-flight rendezvous between the BLPB and the French research aircraft ATR42[8], which was equipped with a UV-absorption ozone analyzer (among many other sensors – Di Biagio et al., 2015).

20 This was especially challenging owing to many constraints in the airspace over the western Mediterranean and the impossibility to control the balloon trajectories. Nevertheless, the aircraft managed to fly as close as possible to the balloons on rare occasions. This was the case on 6 July 2012. Two BLPBs (B08 and B06) were launched from Martigues in the early morning (02:37 and 04:46 UTC, resp.), and followed similar trajectories toward Corsica (Fig.12a). They eventually reached the island in the evening. B06, in particular, approached very close to the Ersa research station, where a UV-absorption ozone analyzer

25 (type Thermo 49i) was operated continuously. The station is situated on a mountain crest at an altitude (533 m asl) close to the balloon flight level (500-550 m asl during the last flight hour).

The different ozone time series are shown in Fig.12(b). Between 03-06 UTC, B08 recorded questionably low ozone mole fractions (data filtered out in Fig.12b). It appeared from the balloon's other data (not shown) that B08 encountered wet conditions and likely condensation which affected the balloon altitude and possibly also the ozonesonde (*e.g.,* water dropplets

30 sucked in the pump). After sunrise however, B08 seemed to again provide reliable data.

---

[8]SAFIRE research service: http://www.safire.fr.

First, it is interesting to see that B06 and B08 stayed close to each other all their way (horizontally – less than 30 km – as well as vertically – Fig.12b), and that their ozone time series are in fairly good agreement. A second validation element is the consistency of the BLPB data with the aircraft measurements, especially during the rendezvous of the aircraft flight #27, when the aircraft flew very close to B06 (balloon in eye contact, as reported by the aircraft passengers). Lastly, ozone data from B06

5   and the Ersa surface station fairly agree by the end of B06 flight (around 20 UTC) when the balloon got close to the station.

Another interesting case for validation purpose is BLPB flight B61 on 29-30 July 2013 during SAFMED (Fig.13). The balloon was launched from Levant island in the evening of 29 July. It flew toward Corsica at levels between 400 and 500 m asl and reached the island west coast after about 3 hours. Then, obviously under the effect of a flow-around regime near the island, the balloon flew northeastward along the coast, experiencing turbulence and strong altitude variations. B61 touched

10   Cape Corsica (the northern tip of the island) around 03:30 UTC. The balloon crossed the mountain chain 7 km south of the Ersa station. Unfortunately, B61 stopped transmitting ozone data after this time, but the balloon nevertheless went on further between Corsica and Italy for 10 hours more (not shown in Fig.13). The ozone surface record at Ersa (Fig.13b) shows a homogeneous air mass all evening and night long, with mole fractions in the range 35-40 ppbv, in fair agreement with B61's ozone record.

15   In conclusion from these comparisons, the BLPB ozonesondes proved their ability to provide ambient ozone mole fractions over the Mediterranean with an accuracy of about 10%.

4.3 General findings on ozone

Ozone levels recorded over sea during the BLPB flights are globally in the range 20-80 ppbv (Tab.2 and Fig.10). This range hides a variety of situations with different ozone backgrounds, but a general feature is that relatively weak diurnal varia-

20   tions were observed compared to usual ground-based observations in the summer continental boundary layer (as illustrated in Fig.8a). During a given BLPB flight, the amplitude of ozone change generally did not exceed 20 ppbv[9]. This contrasts also with the results reported by Mao et al. (2006), who investigated the pollution plume transported from New York City over the Atlantic during the 2004 ICARTT campaign, by means of ozone sensors aboard "smart balloons" (a type of constant volume balloons used by this research group). They found high spatial and temporal ozone variability in the pollution plume at low

25   level (~500 m) over the ocean (*e.g.,* variations exceeding 80 ppbv within 10 km and 15 min). They attributed this variability to the patchiness of the ozone field in the plume, where small pockets of high concentrations could result from a combination of factors including strong daytime ozone photoproduction and transport at small-scale.

Such variability was obviously not reported by our BPLB ozone measurements over the Mediterranean during the three ChArMEx campaigns. An explanation could be that no major ozone pollution episode was actually encountered during these

30   campaigns, contrasting with the situations investigated during ICARTT. Despite this, evidence of ozone photochemistry over the Mediterranean could be found during some BLPB flights.

Bénech et al. (2008) investigated whether Lagrangian photochemical ozone production can be evidenced and quantified from constant volume balloon (CVB) measurements carried out in 2000 and 2001 during the ESCOMPTE project. The authors

---

[9]Greater amplitudes are reported in Tab. 2 for some flights, but the reported values include outliers.

identified CVB trajectory sections in which the considered balloon drifted obviously inside the same air mass. Ozone change in this air mass might be due to ozone chemistry, but also to vertical turbulent transport. The latter might be strong especially near the top of the boundary layer, where large vertical gradients of ozone and other atmospheric species – especially water vapor – are often encountered. An ozone trend in this case is likely to coincide with a trend in specific humidity as well. Conversely, constant specific humidity is an indication that the balloon flew in a well-mixed air mass, and ozone change in this case is more likely related to in situ chemistry.

Such an analysis has been conducted based on the ozone and specific humidity time series from the 2012-2013 BLPB flights. Ozone trends during daytime over intervals of at least 4 hours were observed for 12 flights out of 16 (Tab.2). Ozone mole fraction increased in a majority of cases (9 out of 16). No obvious trend was found in 4 cases. Ozone decrease was observed in three cases (B57, B65, B69).

For 7 flights (namely B06, B08, B10, B55, B57, B59 and B62), specific humidity was found almost constant over the considered time intervals and therefore the ozone trend can be likely attributed to ozone chemistry. Among these flights, 6 showed ozone build-up at rates ranging from 1.2 to 2.2 ppbv h^{-1}. Such values are lower than those reported in Bénech et al. (2008) who found a mean growth rate of +6 ppbv h^{-1} in case of ozone production. During ESCOMPTE, most CVB flights took place in the continental boundary layer. This makes a major difference with over sea flights, since the continental boundary layer is constantly supplied in ozone precursors (nitrogen oxides and volatile organic compounds) from the surface. The Marseilles area is especially favourable to ozone production. The CVBs during ESCOMPTE were launched from industrial or urban sites, and likely, the air masses were initially rich in nitrogen oxides. Then the balloon trajectories showed that the air masses were transported over the rural hinterland, where emissions of biogenic volatile organic compounds from the Mediterranean vegetation are strong in summer. This forms the cocktail for explosive ozone production in the boundary layer, as observed by Cros et al. (2004). The 2012 TRAQA and 2013 SAFMED BLPBs were launched from the same area as during ESCOMPTE, but weather conditions were chosen for flights over sea. In such conditions, the initial precursor concentrations in the air mass are potentially similar but then no further supply is expected from the sea surface. This may be an explanation for slower ozone growth in the air mass. Another point is that no major pollution episode was encountered in the area during TRAQA and SAFMED, unlike what was observed during ESCOMPTE, and this might bias the comparison. B63 in the only flight that exhibits rapid ozone increase (+6.5 ppbv h^{-1}) between 12 and 16 h UTC, but this is associated to large specific humidity variations as well as a balloon descent by about 100 m. Hence, it is not obvious to conclude to in situ ozone production. At least part of this growth might be attributed to turbulent transport or to the fact that the balloon sampled different layers in the meantime (the balloon being not Lagrangian along the vertical).

A remarkable case of in situ ozone production was found during flight B55 from Minorca. Even though the ozone growth is relatively slow (+1.2 ppbv h^{-1}), it occurs at high altitude (2400-2500 m). This is presumably the first time that ozone production is evidenced in the free troposphere from direct observation. This flight is presented in more detail in Section 4.4.2.

B57 is the only case of ozone decrease likely related to in situ destruction (in the free troposphere, again). The other two cases of decrease (B65, B69, both at low altitude) are more ambiguous, owing to a larger variability in specific humidity.

4.4 Remarkable flights

4.4.1 Low altitude flight B62

B62 (Fig.14) is an especially interesting flight, which covered almost a full diurnal cycle. Its remarkable trajectory passed between the Corsica and Sardinia islands, and the flight revealed interesting features of the Mediterranean lower troposphere.

5 The specific humidity time-series allows to clearly distinguish 4 flight sections during which it remained roughly constant (Fig.14b). It can be assumed that the balloon sampled the same air mass inside each flight section, and therefore the time evolution of the measured variables can be considered as quasi-Lagrangian.

Flight section 1 occurred in the late night and early morning (B62 launched at 02:59 UTC) and ended around 06:30 UTC. Once the balloon had reached its ceiling altitude, it oscillated between 400 and 500 m asl. The specific humidity also fluctuated

10 between 6 and 8 g kg^{-1}, and, to some extent, mirrored the ozone variations. It may be concluded that the balloon flew in a turbulent air mass where vertical gradients of both humidity and ozone existed – probably near the top of the marine boundary layer. As humidity is likely to decrease with height, and humidity and ozone variations are opposite, higher ozone concentrations are therefore expected in the free troposphere than in the boundary layer. Ozone shows no global trend over flight section 1, therefore no chemical evolution is to be expected.

15 Flight section 2 occurred between 06:30 and 10:40 UTC. This new air mass was significantly moister (11-12 g kg^{-1}) than the previous one. The flight altitude again showed fluctuations but specific humidity remained almost constant, indicating a turbulent well-mixed layer – obviously the marine boundary layer. In the meantime, ozone concentration showed a linear increase of +1.4 ppbv h^{-1}. This is here a clear indication of ozone photochemical production in the marine boundary layer.

By the end of flight section 2, B62 accelerated (from 8 up to 15 m s^{-1} – not shown) while passing between the two islands.

20 This is the evidence of a gap flow acceleration (Venturi effect). In addition, as the flow tended to further accelerate after the point of maximum constriction between the islands, this was here the signature of a supercritical hydraulic flow. This might occur in particular when the lower troposphere acts as a stable two-layer flow, the lower one being the marine boundary layer and the upper one the stable free troposphere, separated by a temperature inversion (*e.g.*, Lesouef et al., 2013, and references therein). A noticeable point is that the layer interface lowers as the lower layer accelerates (owing to conversion of potential

25 into kinetic energy). This can explain the sudden change of air mass at 10:40 UTC shortly after the gap: the quasi-horizontal isopycnic balloon trajectory probably crossed the lowering interface. The sudden decrease of specific humidity (down to 8 g kg^{-1}, Fig.14b), balloon deceleration (Fig.14a), and temperature jump by about 4°C (not shown) support the assumption that the balloon exited from the boundary layer and entered the free troposphere. The temperature jump is also an element supporting the existence of a temperature inversion between the layers.

30 Flight section 3 occurred between 10:40 and 17:50 UTC. During this time the balloon sampled the lower free troposphere, although it flew in the same altitude range than in the previous flight sections. This implies that the marine boundary layer was not as deep as on the other side of Corsica and Sardinia. Ozone increased globally by 0.7 ppbv h^{-1}, at a higher rate during the first 2-3 hours but then more slowly. Here again, this positive trend can be attributed to photochemical ozone production.

During the last flight section 4 in the evening (17:50-20:20 UTC), B62 experienced very moist conditions (specific humidity around 14 g kg^{-1}, relative humidity above 80%), again within the marine boundary layer. The balloon lost progressively its altitude, likely owing to water condensation weighting the balloon. Ozone decrease was observed while specific humidity was relatively constant. However, the balloon descent is significant and the ozone trend might be either linked to a vertical gradient or to ozone chemical destruction. Finally, the balloon went below the critical altitude of 200 m and the flight was aborted.

A numerical simulation covering the B62 flight period was performed by means of the chemistry-transport model MOCA-GE[10] developed by Météo-France (Peuch et al., 1999). The model covers the planetary boundary layer, the free troposphere, and the stratosphere. It provides a number of optional configurations with varying domain geometries and resolutions, as well as chemical and physical parametrization packages (see El Amraoui et al., 2010, 2014). It offers the flexibility to use several chemical schemes for stratospheric and tropospheric studies. The model uses a semi-Lagrangian transport scheme and includes 47 hybrid vertical levels from the surface up to 5 hPa giving the model a vertical resolution between 40 and 400 m in the boundary layer and between 400 m and 800 m in the upper layers.

In this study, MOCAGE is forced dynamically by wind and temperature fields from the ARPEGE model analyses (Courtier et al., 1991). It is run over a regional nested domain (Mediterranean area, see Fig. 15) at a horizontal resolution of 0.2°x0.2° forced by the 2°x2° global domain.

For the global domain, we used the GEIA (Guenther et al., 1995) and the IPCC (Dentener et al., 2005) inventories for natural emissions and anthropogenic emissions, respectively. For the regional domain, we used the MACC II inventory (Kuenen et al., 2011) for the anthropogenic emissions, the GFAS 1.1 product (Kaiser et al., 2012) for biomass burning emissions and the GEIA inventory for the natural emissions.

Figure 15(a) and (b) show the ozone and wind vector fields from MOCAGE approximately at the balloon altitude (950 hPa pressure level) at 06 and 12 UTC, respectively. The balloon was transported offshore from the continent along the northeastern edge of a low-level wind jet locally called mistral. This wind jet is caused by Venturi effect between two mountain massifs in France (Alps and Massif Central) then further accelerates over the sea due to the supercritical nature of the flow (Drobinski et al., 2001). On this day, a branch of the mistral jet was channelled between Corsica and Sardinia, and the balloon was obviously driven in this branch. The model wind field is consistent with the real balloon trajectory (Fig.14a). In the model, ozone increase can be seen in this air mass, caused by in situ photoproduction. The direct comparison of the observed and simulated ozone time series along the (real) balloon trajectory (Fig.15b) reveals a parallel evolution over the course of the day, with a daytime increase of about 10 ppbv. However, the model generates ozone concentrations globally overestimated by about 15 ppbv compared to the observation.

4.4.2 Free-tropospheric flight B55

B55 flight was launched on 2 July 2013 at 18:00 UTC from the Minorca island. The balloon flew east-southeastward for 32 hours in the free troposphere, at altitudes ranging from 2350 to 2480 m asl (Fig.16). It exited from the authorized flight zone while approaching Sicily.

---

[10]MOdèle de Chimie Atmosphérique à Grande Echelle (Large-Scale Chemistry Atmospheric MOdel).

In order to characterize the origin of the air mass sampled by the balloon, a 10-day backward trajectory was computed with the online HYSPLIT model (Draxler and Rolph, 2014; Stein et al., 2015, in press). The trajectory endpoint corresponds to the balloon current position at 21 UTC on 2 July 2013[11]. The trajectory is shown in Fig.16(a). Before passing over Minorca, the air mass had followed a slow anticyclonic trajectory over North Africa, near the surface during the first 6 days, then at altitudes

5 between 2000 and 2800 m during the last 4 days. The model suggests that no major recent anthropogenic influence on the air mass composition is thus to be expected, but aged and diluted residual pollution from the Mediterranean boundary-layer might be present.

The complete day of 3 July 2013 was covered by the balloon measurements. A remarkable ozone increase by more than 25 ppbv was observed during daytime along the flight track, while specific humidity remained relatively constant around 4-5 g

10 kg^{-1}. Again, we defined 4 flight sections for convenience (Fig.16). Section 1 was mostly during the night, with nearly constant ozone mole fraction around 27-28 ppbv. Ozone started then to increase in the early morning at around 03:00 UTC. During a 3-h transition period, both the balloon altitude and the specific humidity varied. Therefore, the cause of the ozone mole fraction increase is not clear for that period.

During flight section 2 in contrast, the specific humidity was remarkably constant (4.7-4.9 g kg^{-1}) while the ozone mole

15 fraction was growing at a rate of 1.0 ppbv h^{-1}. The most likely explanation for ozone increase in this interval is in situ photochemistry. During section 3, ozone variations around the overall trend mirror humidity variations but still, the ozone baseline keeps on growing at about the same rate (1.0 ppbv h^{-1}). During the final nighttime section 4, ozone shows no obvious trend.

To our knowledge, such a direct and continuous Lagrangian observation of ozone photoproduction in the free troposphere

20 has not been reported previously. This case study deserves further work, especially with numerical modelling, to give more support to this hypothesis and specify the chemical mechanism into play.

5 Summary and future work

A specific adaptation of electrochemical concentration cell (ECC) ozonesonde has been developed for long-duration isopycnic flights in the lower atmosphere aboard the last generation of boundary-layer pressurized balloons (BLPBs) – small constant-

25 volume balloons developed by CNES. The main challenge to face was the relatively short lifetime of conventional ECC ozonesondes. Wheras BLPBs can fly and transmit data for days or even weeks, the worktime of ECC ozonesondes is limited to few hours, chiefly owing to electrolyte evaporation in the cathode chamber. The adopted strategy was to save electrolyte by alternating short working phases (pump motor on) and longer rest periods (pump motor off).

The adaptation consists of an entirely new electronic implementation of existing elements from commercial ECC En-Sci "Z"

30 sondes, namely: motor, pump and electrochemical cell. The major specific feature of the new electronic card is that the pump

---

[11]Control parameters used for the HYSPLIT simulation: trajectory endpoint at 39.912260°N, 4.563480°E, 2400 m asl on 2 July 2013, 21 UTC; global REANALYSIS archive used for meteorological fields (details available on https://www.ready.noaa.gov/gbl_reanalysis.php); model vertical velocity used for vertical motion calculation.

motor can be switched on or off following a programmable sequence composed of three steps: (i) a spin-up period (motor on), (ii) a measurement period (motor still on) and (iii) a rest period (motor off). Laboratory tests presented in this article show that a 1-min spin-up period is sufficient to reach stabilized ozone measurement – consistent with the typical response time of ECC sondes to an ozone step, which is of a few tens of seconds. The durations of the measurement period (typically 1-2 min) and

5 of the rest period (such that the overall 3-step sequence is typically 15 to 30 min) can be adjusted to consume the electrolyte more or less rapidly, depending on the expected flight duration and desired sampling rate.

Among other laboratory tests, an outdoor ground-based experiment was conducted over several days in order to evaluate the new ozonesonde performance against the data from a UV absorption analyzer considered as reference. With spin-up and measurement periods of 1 minute each and an overall sequence of 15 min, the ozonesonde provided data within $\pm 10\%$ from

10 the reference during more than 4 days, capturing well several pronounced ozone diurnal cycles (in the range $\sim$0-60 ppbv) as well as features at shorter timescale. The obtained agreement is within the expected absolute accuracy of ECC ozonesonde data in the troposphere (10%, according to the GAW ASOPOS panel, 2011).

The new ozonesonde was then carried out over the western Mediterranean aboard 16 BLPB flights during three campaigns in summer 2012 and 2013. Two launch bases were located on the French Mediterranean coast in the Marseilles area, and a

15 third one on the Minorca island. Drifting altitudes were in the range 0.25-3.2 km. The longest flight lasted more than 32 hours and covered more than 1000 km from Minorca to the south of Malta.

Few other data available from the campaigns (aircraft or ground-based UV analyzer measurements) were suitable for in-flight validation. They all show reasonable agreement with the BLPB ozone data.

Prior to us, Bénech et al. (2008) considered ozonesonde measurements from low-altitude isopycnic balloons launched in

20 2000 and 2001 from the Marseilles area (at that time, standard ECC ozonesonde were used, over much shorter flight durations). Following the method used by these authors, we also identified flight segments, where specific humidity remained nearly constant – an indication that the balloon flew for some time within the same homogeneous air mass, and therefore that the ozone measurement can be considered as quasi-Lagrangian with good confidence. In such cases, the observed ozone trend can be attributed with good confidence to ozone chemistry. In a majority of cases, the ozone mole fraction was found to increase

25 during daytime, with growth rates in the range 1-2 ppbv h^{-1}. This is significatively less than the mean growth rate found by Bénech et al. (2008) (6 ppbv h^{-1}), but in our case, the flights were all over sea, whereas their results were obtained mainly over land. Moreover, several major pollution episodes were experienced during the 2000-2001 campaigns, but this was not the case in 2012-2013.

Beyond the overview presented in this article, several interesting flights deserve to be investigated in more detail, especially

30 paying more attention to other experimental data from the 2012-2013 campaigns as well as chemistry-transport numerical simulations. Among these flights, one (B55) flew in the free troposphere (around 3000 m above sea level) and revealed ozone growth by about 1 ppbv h^{-1} during daytime, while specific humidity remained nearly constant. This is potentially the first observation of ozone photoproduction in the free troposphere with a direct and continuous Lagrangian point of view. However, further work is needed to confirm this result and study the cause of the observed evolution.

From a technical point of view, an interesting evolution of the BLPB ozonesonde (and potentially also of conventional ECC sondes) would be the onboard measurement of the pump flow rate. Indeed, the ozone current measured in the ECC is proportional to the pump flow rate. From laboratory tests we made, it was found to vary by 1-2% during the first three minutes after the pump motor has been turned on. This could reduce partly the uncertainty associated to the ozone measurement.

5 However, the major uncertainty source for tropospheric ozone measurements is related to the sonde background current (i.e. the current measured in absence of ozone). This is a general concern for all types of ECC ozonesondes and reducing this source of uncertainty remains an open research challenge (Vömel and Diaz, 2010; GAW ASOPOS panel, 2011).

Appendix A: ECC ozonesonde theory and data processing

A1   Theory

10 ECC ozone sensors consist of two teflon chambers equipped with platinum electrodes and containing KI solutions at different concentrations. The two chambers serve as anode and cathode, linked with an ion bridge to allow electrical conduction. The platinum electrodes are connected through an external circuit including a microammeter.

The cathode half-reaction involves the iodide/iodine redox couple (I^-/I_2), whereas the iodide/triiodide couple (I^-/I_3^-) is to consider at the anode. When both electrodes are electrically connected through an external circuit, a current surge occurs

15 until a new equilibrium state is reached, such that concentrations in I^-, I_2 and I_3^- realize matching electrode Nernst potentials (Komhyr, 1969). The ozone sensor works from this equilibrium state.

One major feature of an ECC ozonesonde is a teflon pump that sucks ambient air potentially containing ozone, and makes it bubble into the cathode solution at constant volumic flow rate Q_v. In the cathode chamber, a iodine molecule is produced per ozone molecule oxidizing two I^- ions:

20 $$2KI + O_3 + H_2O \rightarrow 2KOH + I_2 + O_2. \tag{AR1}$$

To restore the equilibrium state, the iodine molecule in excess is consumed at the cathode:

$$I_2 + 2e^- \rightarrow 2I^-. \tag{AR2}$$

This requires two electrons that are given by the anode:

$$3I^- \rightarrow I_3^- + 2e^-. \tag{AR3}$$

25 As a result, a current of two electrons is produced per ozone molecule reduced in the cathode solution. If reaction AR1 is assumed to be rapid and total, the current in the circuit (I_{O_3}) is therefore in proportion of the ozone concentration in air ($[O_3]$ in mol m^{-3}) multiplied by a conversion efficiency factor η:

$$I_{O_3} = 2F[O_3]\eta Q_v, \tag{A1}$$

where F is the Faraday constant (charge of one mole of electrons). The conversion efficiency η is the ratio of ozone molecules in air that are absorbed into the cathode solution and react with iodide ions (AR1)[12]. It is usually assumed that η is nearly unity at neutral pH (Smit et al., 2007; GAW ASOPOS panel, 2011) – the reason why a pH buffer is added to the KI solution (App.B1).

5   Note however that in absence of ozone in air, a residual current is nevertheless measured in cell, which is known as *background current*, and noted I_0. The origin of this current is still under debate, and is discussed in Vömel and Diaz (2010); GAW ASOPOS panel (2011) and references therein. The background current is usually measured connecting the sonde inlet to a zero air generator or an ozone destructor filter. The ozone current is finally $I_{O_3} = I - I_0$ where I is the total current measured through the cell.

10   The ozone partial pressure in air is obtained from the concentration: $P_{O_3} = [O_3]RT$, where R is the universal gas constant and T the absolute temperature of air (measured in the pump body). The ozone mole fraction $x_{O_3} = P_{O_3}/P$ (P being ambient pressure) finally reads:

$$x_{O_3} = \frac{R}{2F} \frac{T}{P} \frac{I - I_0}{\eta Q_v}. \tag{A2}$$

T, I and P are directly measured on board during the flight, while I_0 and Q_v are estimated before the flight and considered
15   as constant parameters.

A2   Data processing

The method used in this study for calculation of ozone mole fractions from measurements (data processing) is detailed below. The required input data are:

- I_0: background current estimated during the pre-flight preparation or from independent surface ozone data,

20   - P_0: ground pressure – measured during the pre-flight preparation,

- t_p: pump time of a reference volume of air $V_0 =$ 100 ml – measured during the pre-flight preparation,

- I: ECC cell current – measured in-flight,

- P: ambient pressure – measured in-flight,

- T: pump temperature – measured in-flight.

25 ## A2.1   Background current correction

Following Komhyr (1969) and until recently, many authors have assumed that the background current measured in ECC sondes is caused by a small interference by oxygen reacting with KI, and therefore that it is dependent on ambient pressure

---

[12]Note that η has here the same definition as in GAW ASOPOS panel (2011) but is the inverse quantity as the coefficient used in Smit et al. (2007).

and decreases with altitude (*e.g.,* Smit et al., 2007). In turn, data processing methods often consider more or less sophisticated pressure-dependent corrections to the background current measured (at the ground level) during the pre-flight preparation.

However, recent studies do not confirm the assumption of oxygen interference, but stress that the background current is related to past ozone exposure and could be the result of a slow reaction pathway of ozone in the cathode solution with

5   a time-constant typically of 20-30 min (Vömel and Diaz, 2010; GAW ASOPOS panel, 2011). The latter panel of experts acknowledges that the understanding of the background current in ECC sondes is still poor, and recommends to use a constant, pressure independent, background current value throughout the entire vertical profile in GAW sounding stations.

We have followed this recommendation in the present study, and for each balloon flight, we used a constant value of I_0 whatever the balloon altitude.

10   **A2.2   Pump-flow correction**

A ground-level value of the pump flow rate Q_v (noted Q_{v0}) is measured by means of a soap bubble flowmeter, as the time t_p needed to pump a reference volume V_0 (usually 100 ml), so that $Q_{v0} = V_0/t_p$.

However, the pump flow rate is known to decline with decreasing pressure (Smit et al., 2007; GAW ASOPOS panel, 2011). A pressure-dependent factor $C(P)$ is applied to correct the decrease in pump efficiency at reduced pressure:

$$Q_v(P) = \frac{Q_{v0}}{C(P)} = \frac{V_0}{C(P)\,t_p}.$$

$C(P)$ is obtained as a polynomial fit of experimental values provided by the manufacturer (Droplet Measurement Technologies, Inc.) and reported in Tab.3:

15    $C(P) = b_0 + b_1 l_P + b_2 l_P^2 + b_3 l_P^3 + b_5 l_P^5,$ (A3)

where $l_P = log_{10}(P)$ (in hPa). The polynom coefficient values are listed in Tab.4.

Note that all BLPB flights considered in this study were below 700 hPa, and thus the applied pump flow corrections were negligible (see Tab.3).

A2.3   Ozone mole fraction final calculation

20   Using the above pressure dependent expressions for $I_0(P)$ and $Q_v(P)$ and assuming the conversion efficiency $\eta = 1$, Eq.A2 finally reads:

$$x_{O_3} = \frac{R}{2F} \frac{T}{P} \frac{C(P)}{V_0} t_p (I - I_0(P)),$$ (A4)

where $R = 8.31$ J K^{-1} mol^{-1} and $F = 96485$ C mol^{-1}.

Appendix B: ECC ozonesonde operation

B1 Anode and cathode solutions

The "0.5% half-buffer" (Smit et al., 2007) cathode solution used in this study is composed (per litre of solution) of

- 5.000 g of KI (i.e. approximately 0.5% in mass),

- 12.500 g of KBr,

- a pH buffer composed of 0.630 g of $NaH_2PO_4.H_2O$ and 2.500 g of $Na_2HPO_4.12H_2O$.

The KI-saturated anode solution was obtained taking 50 ml of cathode solution and adding 70 g of KI.
VWR NORMAPUR® chemicals were used to prepare the solutions.

B2 Pre-flight sonde preparation and control

To a large extent, we followed the GAW recommendations for ECC sonde preparation (GAW ASOPOS panel, 2011). We recall here briefly the main steps of our preparation procedure, and point a number of specific adjustments and additional measurements.

B2.1 Advanced sonde preparation

The GAW recommendation is to make the advanced preparation 3-7 days before flight. This is suited for regular (*e.g.,* weekly) soundings. During the 2012 and 2013 campaigns, intensive observation periods (IOP) were triggered upon meteorological alert. During an IOP, up to 6 ozonesondes were launched within 24h. A great number of sondes had to be prepared without visibility on the flight date. Consequently, the advanced preparations were sometimes made from 2 to 14 days before flight.

The main steps of the advanced preparation were:

- checking motor and pump performance,

- conditioning of the tubing, pump body and cathode chamber under high concentration of ozone for 30 minutes,

- flushing with clean zero ozone air for few minutes,

- filling the cathode and anode chambers with solutions,

- running the sonde for 15-30 minutes with clean zero ozone air to allow the background current to drop below 0.5 μA,

- running the sonde for 10 minutes with ozonized air so that the current stabilizes in the range of 5-6 μA,

- running the sonde for 10 minutes with clean zero ozone air.

B2.2 Flight day sonde preparation

This preparation was made few hours before flight. The main steps were:

- conditioning the pump (only) under high concentration of ozone for 10-20 minutes then flushing with zero ozone air for few minutes,

- recharge the anode and cathode chambers with fresh solutions,

- running the sonde for 15-30 minutes with clean zero ozone air, then measuring the background current I_0,

- running the sonde for 10 minutes with ozonized air so that the current stabilizes in the range of 5-6 μA, and measuring the pump flow time t_p in the meanwhile,

- checking that $(I - I_0) \times t_p$ (which is proportional to ozone concentration, Eq.A4) matches within 5% against a reference
10 ECC sonde (same ozonizer tuning),

- checking that the current drops by 70-80% in one minute after having turned the ozonizer off,

- running the sonde for 10 extra minutes with clean zero ozone air.

B2.3 Final preparation, additional measurements and retained background current values

During the final preparation (1-2 hours before flight), the background current and the pump flow rate were again measured
15 carefully, as recommended in the GAW standard operation procedure (GAW ASOPOS panel, 2011).

For the 2012 campaign, additional calibration data are available whereby the sonde pumped air from an ozone calibrator (Ansyco KT-O3M) with scale points at 1.4, 56 and 106 ppbv. In this case, the values of the background current and pump flow rate used for data processing were adjusted such that the derived ozone mole fractions fit at best the calibrator scale points.

Unfortunaltely, no such calibration data are available for the 2013 campaigns. Nevertheless, surface ozone was being con-
20 tinuously measured on the launch site (by means of a TEI 49i UV-absorption ozone analyzer). Unlike in 2012, the BLPB ozonesondes worked in continuous mode during the launch and balloon ascent phases, enabling to measure vertical profiles from the ground up to the BLPB ceiling level. In such case, the I_0 value was adjusted such that the lowest data point from the ascent profile matches the analyzer ozone reading at launch time (Fig.11). The same was done to process data from the conventional radiosoundings with ECC ozonesondes.

25 The only exception was the BLPB flight B55 (in 2013). The ozone data during the launch and ascent phases were obviously not valid (possibly perturbed by very high humidity in the lowest troposphere). Thus, the vertical profile was not used to estimate I_0, but instead the ground-based measurement of I_0 during the final preparation phase was retained (as it is conventionally done in most sounding stations).

Acknowledgements. The ozone BLPB project was supported and funded by the French space agency CNES, and also by the French national research institute CNRS/INSU through its research programme MISTRALS/ChArMEx. The TRAQA campaign was partly supported by ADEME (French environment and energy management agency). We gratefully thank all members of the CNES technical staff, who brought a priceless support during and around the field campaigns, as well as the SEDOO group of the Observatoire Midi-Pyrénées who made

5   available the forecast trajectories used to decide the BLPB launches. The authors also acknowledge the NOAA Air Resources Laboratory (ARL) for the provision of the HYSPLIT transport and dispersion model and READY website (http://www.ready.noaa.gov) used in this publication.

References

Bénech, B., Durand, P., and Druilhet, A.: A case-study of a non-homogeneous boundary layer (AUTAN 84 experiment), Annal. Geophys. B, 5, 451–460, 1987.

Bénech, B., Ezcurra, A., Lothon, M., Said, F., Campistron, B., Lohou, F., and Durand, P.: Constant volume balloons measurements in the urban Marseille and Fos-Berre industrial ozone plumes during ESCOMPTE experiment, Atmospheric Environment, 42, 5589–5601, doi:10.1016/j.atmosenv.2008.03.011, 2008.

Businger, S., Chiswell, S., Ulmer, W., and Johnson, R.: Balloons as a Lagrangian measurement platform for atmospheric research, J. Geophys. Res., 101, 4363–4376, 1996.

Businger, S., Johnson, R., and Talbot, R.: Scientific insights, Bull. Am. Meteor. Soc., 87, 1539–1554, doi:10.1175/BAMS-87-11-1539, 2006.

Caccia, J.-L., Bénech, B., and Klaus, V.: Space-time description of nonstationary trapped lee wave using ST radars, aircraft and constant volume balloons during the PYREX experiment, J. Atmos. Sci., 54, 1821–1883, 1997.

Cadet, D., Ovarlez, H., and Ovarlez, J.: Superpressure balloon flights in the tropical boudary layer, J. Appl. Meteor., 14, 1478–1484, 1975.

Cadet, D., Ovarlez, H., and Sommeria, G.: The BALSAMINE experiment during the summer MONEX, Bull. Am. Meteor. Soc., 62, 381–388, 1981.

Courtier, P., Freydier, C., Geleyn, J., Rabier, F., and Rochas, M.: The ARPEGE project at Météo France, Atmospheric Models, Workshop on Numerical Methods, Reading, U.K., 2, 193–231, 1991.

Cros, B., Durand, P., Cachier, H., Drobinski, P., Frejafon, E., Kottmeïer, C., Perros, P., Peuch, V.-H., Ponche, J., Robin, D., Saïd, F., G., T., and Wortham, H.: The ESCOMPTE program: an overview, Atmospheric Research, 69, 241–279, 2004.

Cuesta, J., Eremenko, M., Liu, X., Dufour, G., Cai, Z., Höpfner, M., von Clarmann, T., Sellitto, P., Foret, G., Gaubert, B., Beekmann, M., Orphal, J., Chance, K., Spurr, R., and Flaud, J.-M.: Satellite observation of lowermost tropospheric ozone by multispectral synergism of IASI thermal infrared and GOME-2 ultraviolet measurements over Europe, Atmos. Chem. Phys., 13, 9675–9693, doi:10.5194/acp-13-9675-2013, 2013.

Dentener, F., Stevenson, D., Cofala, J., Mechler, R., Amann, M., Bergamaschi, P., Raes, F., and Derwent, R.: The impact of air pollutant and methane emission controls on tropospheric ozone and radiative forcing: CTM calculations for the period 1990-2030, Atmos. Chem. Phys., 5, 1731–1755, 2005.

Deshler, T., Mercer, J., Smit, H., Stuebi, R., Levrat, G., Johnson, B., Oltmans, S., Kivi, R., Thompson, A., Witte, J., Davies, J., Schmidlin, F., Brothers, G., and Sasaki, T.: Atmospheric comparison of electrochemical cell ozonesondes from different manufacturers, and with different cathode solution strengths: The Balloon Experiment on Standards for Ozonesondes, J. Geophys. Res., 113, D04 307, doi:10.1029/2007JD008975, 2008.

Di Biagio, C., Doppler, L., Gaimoz, C., Grand, N., Ancellet, G., Raut, J.-C., Beekmann, M., Borbon, A., Sartelet, K., Attié, J.-L., Ravetta, F., and Formenti, P.: Continental pollution in the western Mediterranean basin: vertical profiles of aerosol and trace gases measured over the sea during TRAQA 2012 and SAFMED 2013, Atmos. Chem. Phys., 15, 9611–9630, doi:10.5194/acp-15-9611-2015, 2015.

Draxler, R. and Rolph, G.: HYSPLIT (HYbrid Single-Particle Lagrangian Integrated Trajectory) Model access via NOAA ARL READY Website (http://www.arl.noaa.gov/HYSPLIT.php), NOAA Air Resources Laboratory, College Park, MD, USA, 2014.

Drobinski, P., Flamant, C., Dusek, J., Flamant, P., and Pelon, J.: Observational evidence and modelling of an internal hydraulic jump at the atmospheric boundary-layer top during a tramontane event, Boundary-Layer Meteorology, 98, 497–515, 2001.

Durand, P., Druilhet, A., Bénech, B., and Hammam, A.: Mean and turbulent structure of a non-homogeneous boundary layer: experimental study of two local winds during AUTAN 84, Annal. Geophys., 11, 502–517, 1993.

El Amraoui, L., Attié, J.-L., Semane, N., Claeyman, M., Peuch, V.-H., Warner, J., Ricaud, P., Cammas, J.-P., Piacentini, A., Josse, B., Cariolle, D., Massart, S., and Bencherif, H.: Midlatitude stratosphere–troposphere exchange as diagnosed by MLS O3 and MOPITT CO assimilated fields, Atmos. Chem. Phys., 10, 2175–2194, doi:doi:10.5194/acp-10-2175-2010, 2010.

El Amraoui, L., Attié, J.-L., Ricaud, P., Lahoz, W., Piacentini, A., Peuch, V.-H., Warner, J., Abida, R., and Barré, J.: Tropospheric CO vertical profiles deduced from total columns using data assimilation: methodology and validation, Atmos. Meas. Tech., 7, 3035–3057, doi:doi:10.5194/amt-7-3035-2014, 2014.

Ethé, C., Basdevant, C., Sadourny, R., Appu, K., Harenduprakash, L., Sarode, P., and Viswanathan, G.: Air mass motion, temperature and humidity over the Arabian Sea and western Indian Ocean during the INDOEX intensive phase, as obtained from a set of superpressure drifting balloons, J. Geophys. Res., 107 (D19), 8023, doi:10.1029/2001JD001120, 2002.

GAW ASOPOS panel: Quality assurance and quality control for ozonesonde measurements in GAW - GAW Report no.201, p. pp.92, World Meteorological Organization, Geneva, Switzerland, http://www.wmo.int/pages/prog/arep/gaw/documents/GAW_201.pdf, 2011.

Gheusi, F., Ravetta, F., Delbarre, H., Tsamalis, C., Chevalier-Rosso, A., Leroy, C., Augustin, P., Delmas, R., Ancellet, G., Athier, G., Bouchou, P., Campistron, B., Cousin, J.-M., Fourmentin, M., and Meyerfeld, Y.: Pic 2005, a field campaign to investigate low-tropospheric ozone variability in the Pyrenees, Atmospheric Research, 101, 640–665, doi:10.1016/j.atmosres.2011.04.014, 2011.

Gifford, F.: A simultaneous Lagrangian–Eulerian turbulence experiment, Mon. Wea. Rev., 83, 293–301, 1955.

Guenther, A., Hewitt, C. N., Erickson, D., Fall, R., Geron, C., Graedel, T., Harley, P., Klinger, L., Lerdau, M., McKay, W., et al.: A global model of natural volatile organic compound emissions, Journal of Geophysical Research: Atmospheres (1984–2012), 100, 8873–8892, 1995.

Kaiser, J., Heil, A., Andreae, M., Benedetti, A., Chubarova, N., Jones, L., Morcrette, J.-J., Razinger, M., Schultz, M., Suttie, M., et al.: Biomass burning emissions estimated with a global fire assimilation system based on observed fire radiative power, Biogeosciences, 9, 527–554, 2012.

Koffi, E., Georgelin, M., Bénech, B., and Richard, E.: Trapped lee waves observed during PYREX by constant volume balloons: comparison with Meso-NH simulations, J. Atmos. Sci., 57, 2007–2021, 2000.

Komhyr, W.: Electrochemical concentration cells for gas analysis, Annales de Géophysique, 25, 203–210, 1969.

Kuenen, J., Denier van der Gon, H., Visschedijk, A., Van der Brugh, H., and Van Gijlswijk, R.: MACC European emission inventory for the years 2003–2007, TNO-report TNO-060-UT-2011-00588, Utrecht, 2011.

Legain, D., Bousquet, O., Douffet, T., Tzanos, D., Moulin, E., Barrie, J., and Renard, J.-B.: High-frequency boundary layer profiling with reusable radiosondes, Atmos. Meas. Tech., 6, 2195–2205, doi:10.5194/amt-6-2195-2013, 2013.

Lesouef, D., Gheusi, F., Chazette, P., Delmas, R., and Sanak, J.: Low tropospheric layers over Reunion Island in lidar-derived observations and a high-resolution model, Boundary-Layer Meteorology, 149, 425–453, doi:10.1007/s10546-013-9851-9, 2013.

Mallet, M., Dulac, F., Formenti, P., Nabat, P., Sciare, J., Roberts, G., Pelon, J., Ancellet, G., Tanré, D., Parol, F., di Sarra, A., Alados, L., Arndt, J., Auriol, F., Blarel, L., Bourrianne, T., Brogniez, G., Chazette, P., Chevaillier, S., Claeys, M., D'Anna, B., Denjean, C., Derimian, Y., Desboeufs, K., Di Iorio, T., Doussin, J.-F., Durand, P., Féron, A., Freney, E., Gaimoz, C., Goloub, P., Gómez-Amo, J. L., Granados-Muñoz, M. J., Grand, N., Hamonou, E., Jankowiak, I., Jeannot, M., Léon, J.-F., Maillé, M., Mailler, S., Meloni, D., Menut, L., Momboisse, G., Nicolas, J., Podvin, J., Pont, V., Rea, G., Renard, J.-B., Roblou, L., Schepanski, K., Schwarzenboeck, A., Sellegri, K., Sicard, M., Solmon, F., Somot, S., Torres, B., Totems, J., Triquet, S., Verdier, N., Verwaerde, C., Wenger, J., and Zapf, P.: Overview of the

Chemistry-Aerosol Mediterranean Experiment/Aerosol Direct Radiative Forcing on the Mediterranean Climate (ChArMEx/ADRIMED) summer 2013 campaign, Atmos. Chem. Phys., 16, 455–504, doi:10.5194/acp-16-455-2016, 2016.

Mao, H., Talbot, R., Troop, D., Johnson, R., Businger, S., and Thompson, A.: Smart balloon observations over the North Atlantic: ozone data analysis and modelling, J. Geophys. Res., 111, D23S56, doi:10.1029/2005JD006507, 2006.

5 Nabat, P., Somot, S., Mallet, M., Chiapello, I., Morcrette, J.-J., Solmon, F., Szopa, S., Dulac, F., Collins, W., Ghan, S., Horowitz, L., Lamarque, J.-F., Lee, Y., Naik, V., Nagashima, T., Shindell, D., and Skeie, R.: A 4-D climatology (1979-2009) of the monthly tropospheric aerosol optical depth distribution over the Mediterranean region from a comparative evaluation and nding of remote sensing and model products, Atmos. Meas. Tech., 6, 1287–1314, doi:10.5194/amt-6-1287-2013, 2013.

Peuch, V.-H., Amodei, M., Barthet, T., Cathala, M. L., Michou, M., and Simon, P.: MOCAGE, MOdèle de Chimie Atmosphérique à Grande
10 Echelle, Proceedings of Météo-France workshop on atmospheric modelling, Toulouse, France, pp. 33–36, 1999.

Renard, J.-B., Dulac, F., Berthet, G., Lurton, T., Vignelles, D., Jégou, F., Tonnelier, T., Thaury, C., Jeannot, M., Couté, B., Akiki, R., Mineau, J.-L., Verdier, N., Mallet, M., Gensdarmes, F., Charpentier, P., Mesmin, S., Duverger, V., Dupont, J.-C., Elias, T., Crenn, V., Sciare, J., Giacomoni, J., Gobbi, M., Hamonou, E., Olafsson, H., Dagsson-Waldhauserova, P., Camy-Peyret, C., Mazel, C., Décamps, T., Piringer, M., Surcin, J., and Daugeron, D.: LOAC: a small aerosol optical counter/sizer for ground-based and balloon measurements of the size
15 distribution and nature of atmospheric particles – Part 1: Principle of measurements and instrument evaluation, Atmos. Meas. Tech. Discuss., 8, 9993–10 056, doi:10.5194/amtd-8-9993-2015, 2015a.

Renard, J.-B., Dulac, F., Berthet, G., Lurton, T., Vignelles, D., Jégou, F., Tonnelier, T., Thaury, C., Jeannot, M., Couté, B., Akiki, R., Mineau, J.-L., Verdier, N., Mallet, M., Gensdarmes, F., Charpentier, P., Mesmin, S., Duverger, V., Dupont, J.-C., Elias, T., Crenn, V., Sciare, J., Giacomoni, J., Gobbi, M., Hamonou, E., Olafsson, H., Dagsson-Waldhauserova, P., Camy-Peyret, C., Mazel, C., Décamps, T., Piringer,
20 M., Surcin, J., and Daugeron, D.: LOAC: a small aerosol optical counter/sizer for ground-based and balloon measurements of the size distribution and nature of atmospheric particles – Part 2: First results from balloon and unmanned aerial vehicle flights, Atmos. Meas. Tech. Discuss., 8, 10 057–10 096, doi:10.5194/amtd-8-10057-2015, 2015b.

Smit, H., Straeter, W., Johnson, B., Oltmans, S., Davies, J., Tarasick, D., Hoegger, B., Stuebi, R., Schmidlin, F., Northam, T., Thompson, A., Witte, J., Boyd, I., and Posny, F.: Assessment of the performance of ECC-ozonesondes under quasi-flight conditions in the environmen-
25 tal simulation chamber: Insights from the Juelich Ozone Sonde Intercomparison Experiment (JOSIE), J. Geophys. Res., 112, D19 306, doi:10.1029/2006JD007308, 2007.

Staehelin, J.: Global atmospheric ozone monitoring, Bull. World Meteor. Org., 57, 45–54, https://www.wmo.int/pages/publications/bulletin_ en/.../ozone_sub.pdf, 2008.

Stein, A., Draxler, R., Rolph, G., Stunder, B., Cohen, M., and Ngan, F.: NOAA's HYSPLIT atmospheric transport and dispersion modeling
30 system, Bull. Am. Meteor. Soc., doi:10.1175/BAMS-D-14-00110.1, 2015, in press.

Vömel, H. and Diaz, K.: Ozone sonde cell current measurements and implications for observations of near-zero ozone concentrations in the tropical upper troposphere, Atmos. Meas. Tech., 3, 495–505, doi:10.5194/amt-3-495-2010, 2010.

Table 1. Launch bases during the 2012 and 2013 campaigns.

Campaign	Period	Launch base	Geo. coord.
TRAQA	25 Jun – 15 Jul 2012	Martigues[a]	43°19.96'N 5°05.22'E
ADRIMED	10 Jun – 6 Jul 2013	Minorca island[b]	39°51.98'N 4°15.30'E
SAFMED	22 Jul – 7 Aug 2013	Levant island[c]	43°01.31'N 6°27.61'E

(a) South-east France, Mediterranean coast. (b) Sant Lluís, Minorca Island, Spain. (c) Island off Hyères, south-east France, Mediterranean coast.

Table 2. Details on the 16 ozone BLPB flights launched during the 2012 and 2013 campaigns. (Note that 13 other BLPB with LOAC payload were also launched during these campaigns (Renard et al., 2015b). Those flights are not in the scope of the present article.)

BLPB flight #	Launch site	Launch date-time (UTC)	Flight duration (h)	Flight range (km)	O_3 record termination (comment[a])	Alt. range at ceiling (m asl)	O_3 range at ceiling (ppbv)	Daytime[b] ozone trend (ppbv h^{-1})	In situ O_3 chemistry (comment[c])
B06	Martigues	2012/07/06 04:46	15.4	371	EXIT	470-609	45-67	+1.6	likely
B08	Martigues	2012/07/06 02:37	15.5	336	EXIT	417-574	02-69	+1.8	likely
B10	Martigues	2012/06/27 01:00	9.5	175	EXIT	566-720	20-46	+2.0	likely
B53	Minorca	2013/06/16 09:56	14.1	193	BLPB	2996-3065	39-44	no	unlikely
B54	Minorca	2013/06/17 09:45	7.0	367	EXIT	1836-2020	36-54	no	unlikely
B55	Minorca	2013/07/02 18:00	32.0	732	EXIT	2429-2477	23-54	+1.2	likely
B57	Minorca	2013/07/02 13:12	33.0	1014	EXIT	3083-3198	49-75	-0.4	likely
B59	Levant	2013/07/22 21:05	15.4	189	EXIT	242-395	45-85	+2.2	likely
B60	Levant	2013/07/25 06:00	19.1	296	EXIT	526-649	54-66	+0.9	not obvious
B61	Levant	2013/07/29 21:56	5.5[d]	279[d]	O_3	300-733	39-42	(night, ≈0)	–
B62	Levant	2013/07/30 02:59	17.4	626	BLPB	207-634	36-48	+1.3	likely
B63	Levant	2013/08/03 06:54	9.9	118	EXIT	467-630	30-53	+6.5	not obvious
B64	Levant	2013/08/03 20:57	21.6	304	EXIT	773-907	39-58	+1.3	not obvious
B65	Levant	2013/08/03 20:57	15.3	299	EXIT	391-615	52-61	-0.7	not obvious
B66	Levant	2013/08/04 02:52	13.3	176	EXIT	798-943	42-59	no	unlikely
B69	Levant	2013/07/25 04:00	19.4	265	BLPB	208-621	41-67	-0.6	not obvious

(a) EXIT = limit of authorized flight zone reached; BLPB = flight aborted owing to balloon failure; O_3 = ozonesonde failure but the flight went on. (b) Maximum trend established over at least 4h between sunrise and sunset. (c) See text for details. (d) These values correspond to the time of the ozone record end, but B61 went on further for about 10 hours and 78 km south-eastwards.

Table 3. Pump-flow correction factor values provided by the En-Sci ECC ozonesonde manufacturer as function of pressure.

Pressure (hPa)	2	3	5	10	20	30	50	100	200	300	500	1000
Correction factor C	1.171	1.131	1.092	1.055	1.032	1.022	1.015	1.011	1.008	1.006	1.004	1

Table 4. Polynom coefficient values (Eq.A3).

b_0	1.2585355012
b_1	-0.3376789017
b_2	0.1627868522
b_3	-0.0293336916
b_5	0.0003347254
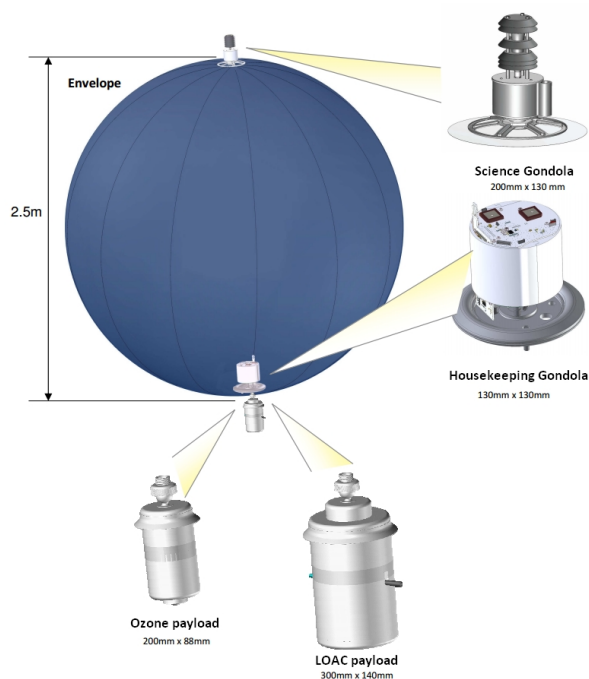
Figure 1. Schematics of a CNES boundary-layer pressurized balloon and its various payloads (2013 version).

Figure 2. Authorized BLPB flight zone over the western Mediterranean (purple shading) during the campaigns of summer 2013. During the 2012 campaign, flights over the Corsica and Sardinia islands were not yet authorized, the rest of the flight zone being the same. The three launch sites used in 2012 and 2013 (namely Martigues, Minorca and Levant, see Section 4) are also indicated in the map.
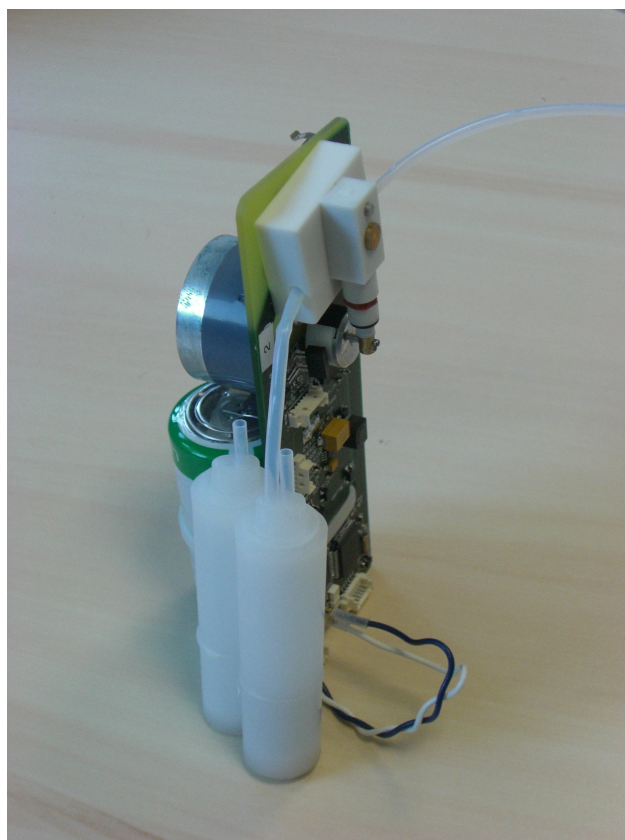
Figure 3. ECC ozonesonde for BLPB (extracted from its polystyrene box – the latter being visible in Fig.1).
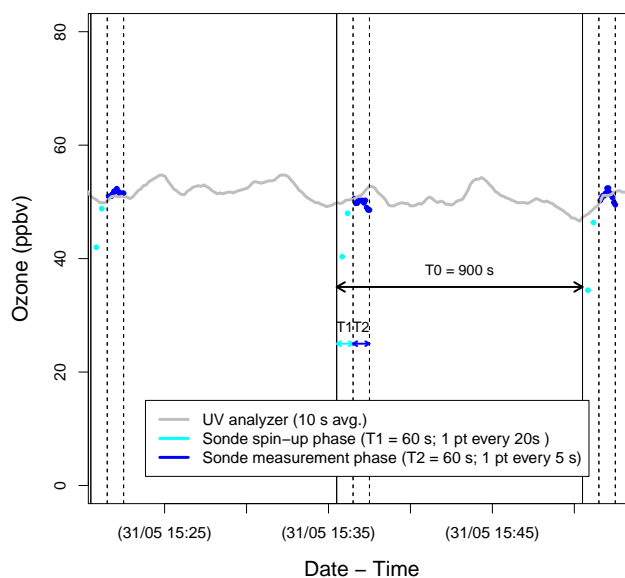
Figure 4. Example (taken from the laboratory test detailed in Sect.3.2) showing 3 measurement cycles of the BLPB ozonesonde. In this illustration, the parameter values are $T_0 = 900$ s, $T_1 = 60$ s and $T_2 = 60$ s.
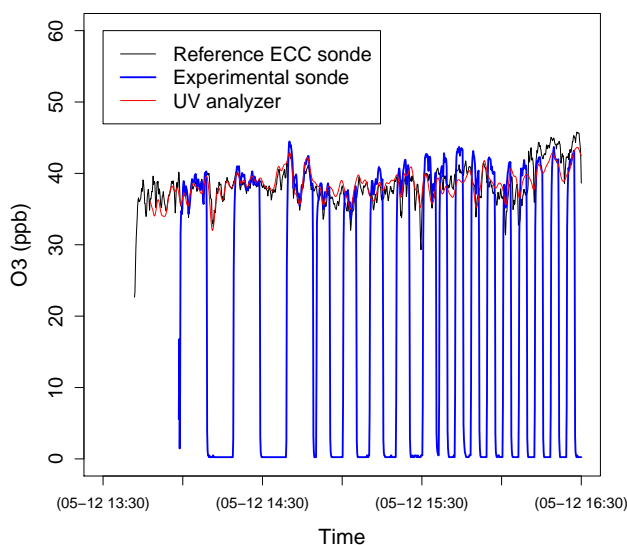
Figure 5. 12 May 2011 ground-based experiment: time series of ozone mole fractions provided by the UV analyzer (red) and retrieved from currents measured in the reference (black) and the experimental (blue) ECC sondes.

(a)   (b)
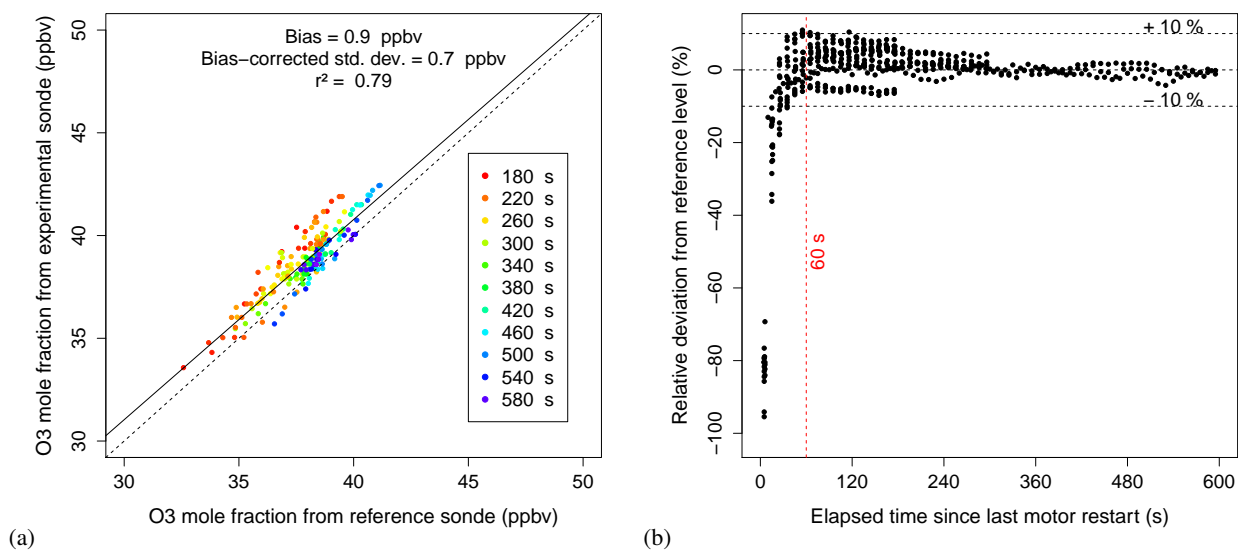
Figure 6. 12 May 2011 ground-based experiment: (a) Comparison between the reference (S_{Ref}) and experimental (S_{Exp}) sondes, but restricted to data between 180 and 600 s of S_{Exp} running since the last motor restart. (b) Deviation of S_{Exp} data from the values predicted by the linear model (in relative value with respect to S_{Ref} data), as function of time elapsed since the last restart of the motor. The red dashed line marks 60 s (spin-up time adopted thereafter). The horizontal dashed lines mark deviations of -10, 0 and +10%.
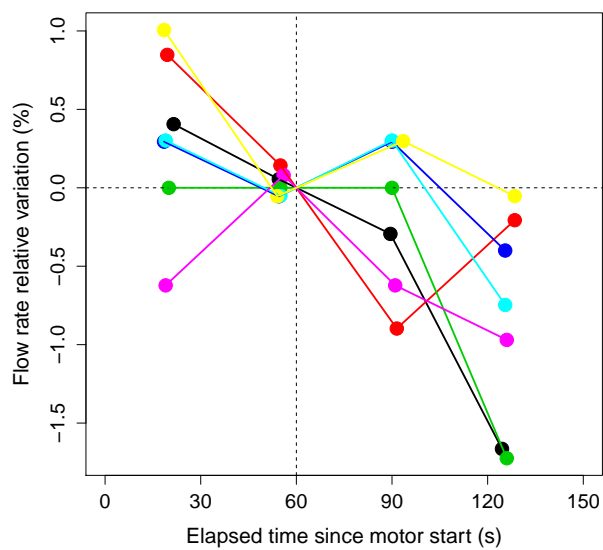
Figure 7. Pump flow rate evolution after sonde motor restart. For each series (differentiated with colors), the values are relative deviations (in %) from the flow rate interpolated at $t = 60$ s after restart ($t = 60$ corresponding to the beginning of the measurement phase).

(a)   (b)
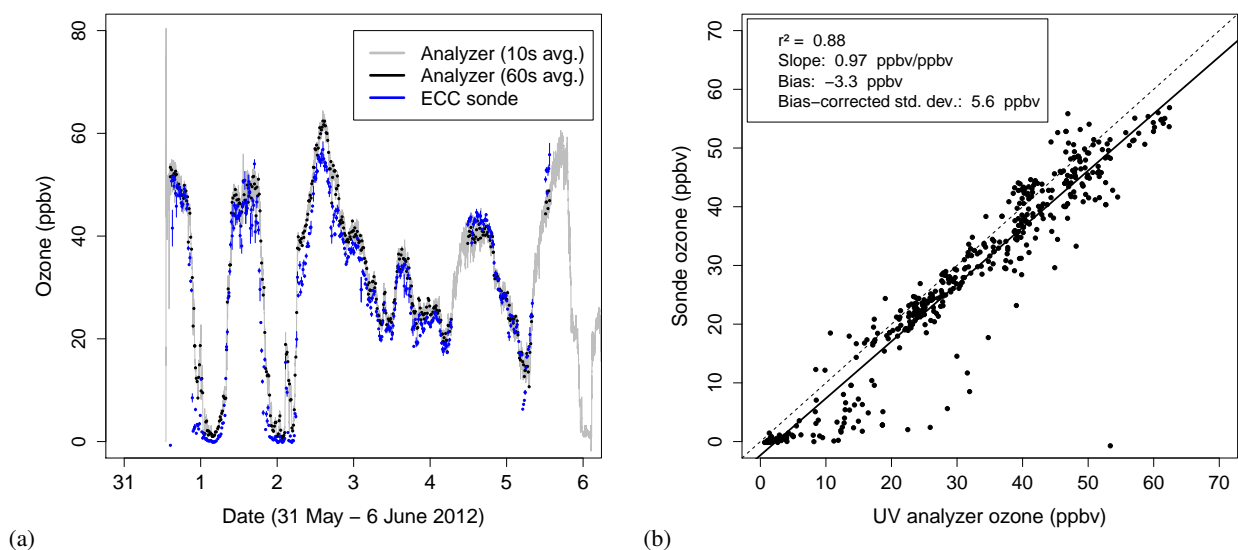
Figure 8. 31 May – 6 June 2012 ground-based experiment: (a) Time series of ozone mole fraction from the UV analyzer (grey curve: 10-s averages (analyzer raw data); black dots: 60-s averages synchronized with the BLPB ozonesonde data) and the BLPB ozonesonde (blue dots; bars represent the standard deviation of the data recorded during each measurement phase). (b) Comparison of the ozone mole fractions from the BLPB ozonesonde against the data from the UV analyzer (synchronized 60-s averages). The numerical results of a linear regression (solid line) are given in the figure panel. The dashed line represents the 1:1 correspondence.

(a) (b)
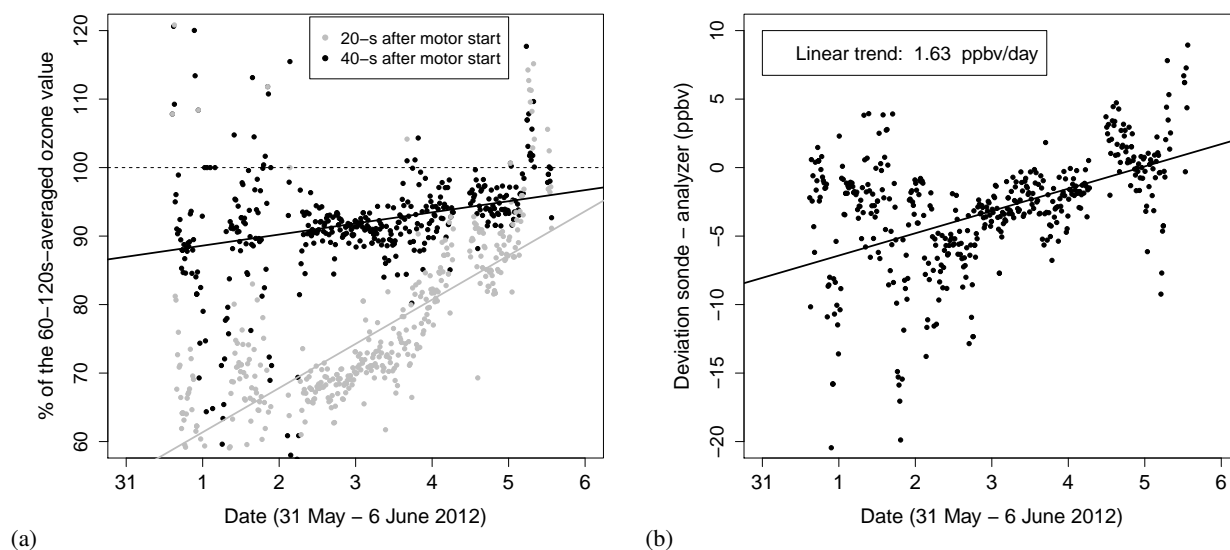
Figure 9. 31 May – 6 June 2012 ground-based experiment: Evolution of the sonde behaviour over its lifetime. (a) Spin-up phase: for each measurement cycle, the represented values are percentages of the eventually established ozone value (see text for detailed definition). Grey dots represent the value measured 20 s after motor start; black dots represent the value measured 40 s after motor start. Lines represent linear regressions over each data set. (b) Deviation of the established ozone value from the UV analyzer as function of time. The line again represents a linear regression.
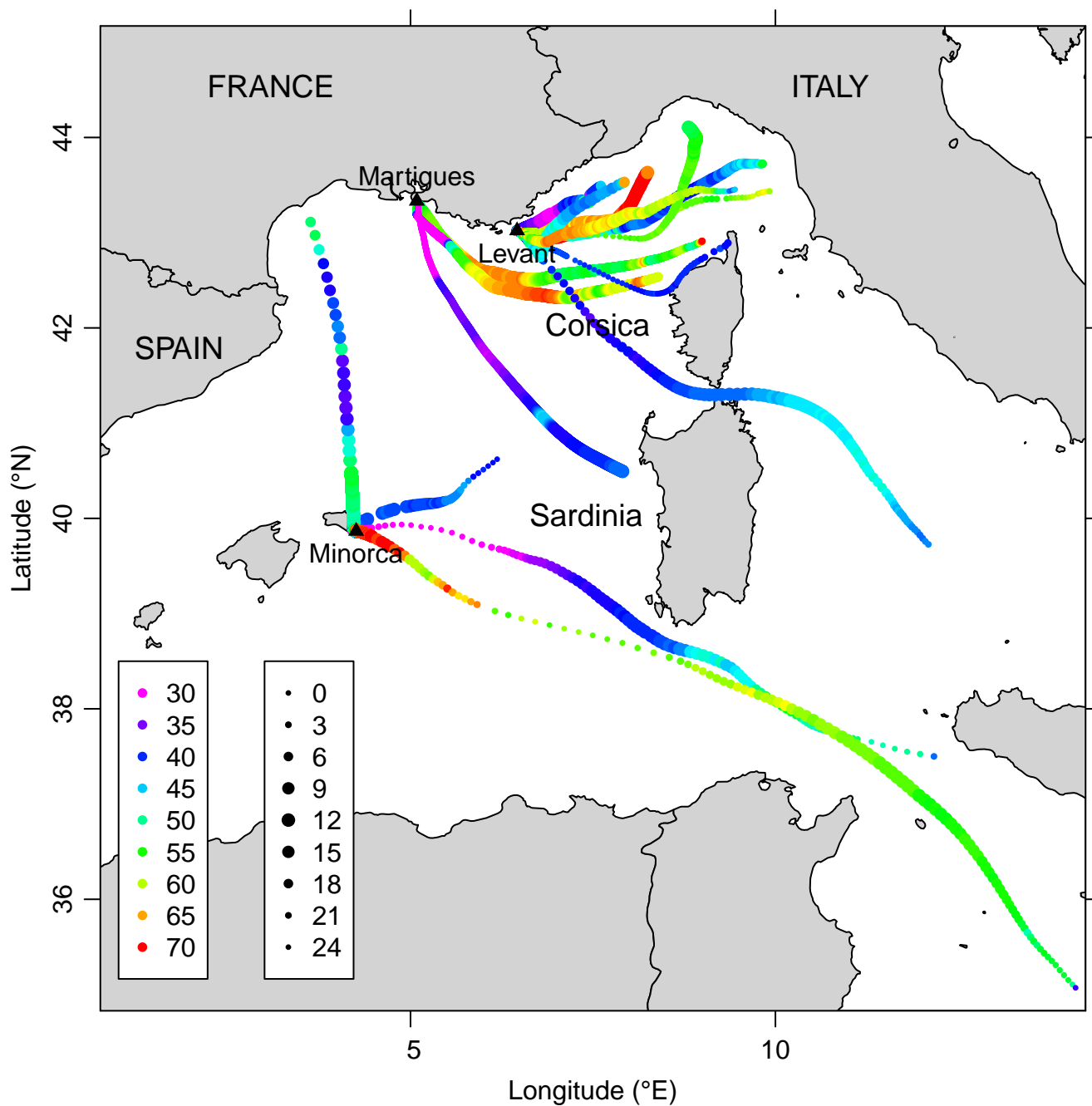
Figure 10. Trajectories of the 16 ozone BLPB flights launched in 2012 and 2013. The color code (left box) represents the ozone mole fraction (in ppbv) measured at each trajectory step. The dot size represents the solar local time (right box).
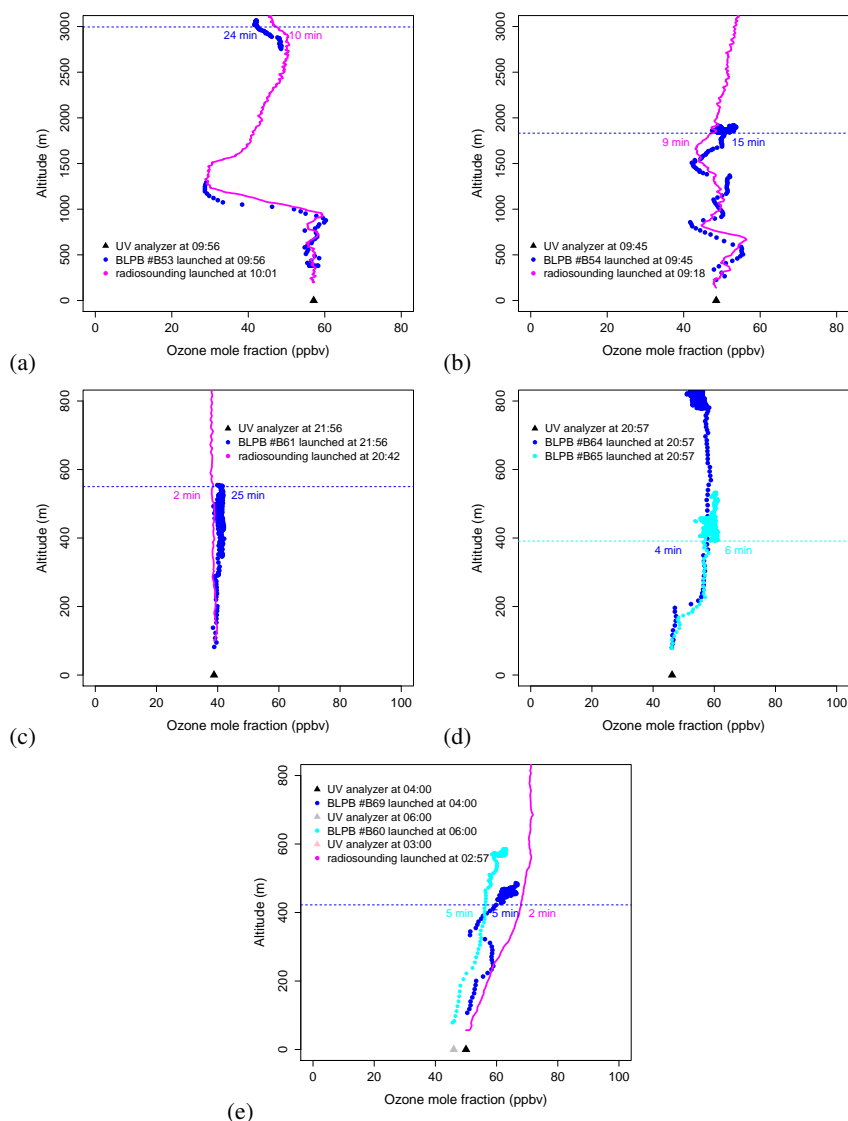
Figure 11. Ozone vertical profiles from radiosoundings and BLPBs during the 2013 campaigns. Note that the altitude scale is not the same in panels (a-b) (3000 m asl) as in panels (c-e) (800 m asl). General to all panels, dots represent BLPB measurements every 10 s (in continuous mode) while radiosounding data are represented as solid lines. The durations (in min) indicated in each panel give the time needed for each balloon to reach the altitude specified by the horizontal dashed line (an estimation of the BLPB ceiling altitude). Triangles represent surface ozone readings (UV analyzer) at the times of BLPB launches. All useful times (UTC) are specified in figure legends.
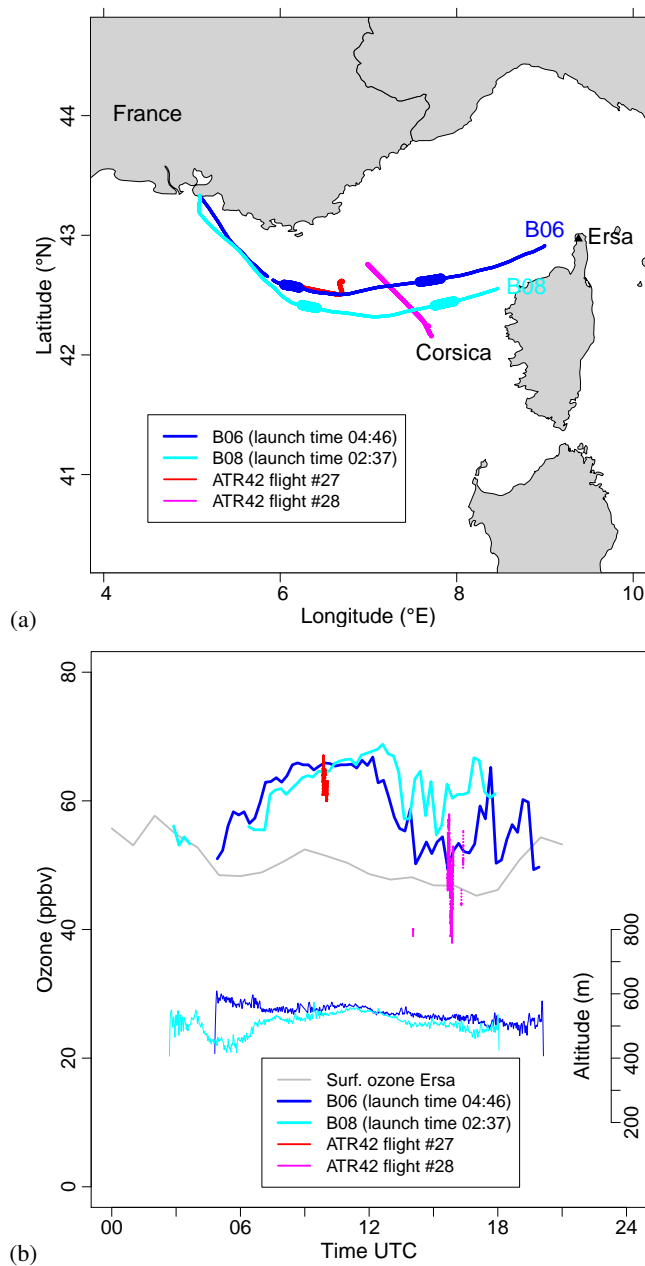
Figure 12. (a) Blue and cyan curves: trajectories of BLPBs B06 and B08 launched from Martigues on 6 July 2012 during TRAQA. Red and magenta curves: sections of the ATR42 research aircraft trajectory during two selected time intervals corresponding to rendezvous with the balloons. The balloon trajectories are broadened during these time intervals in order to indicate their location. (b) Ozone time series on 6 July 2012 from different measurements: BLPBs B06 and B08 (blue and cyan thick curves); ATR42 aircraft at the time of the rendezvous (red and magenta curves); Ersa station surface measurements at 533 m asl (grey curve). The station location is indicated in panel (a). The balloon altitude is also represented as thin curves (same color code and right hand scale).
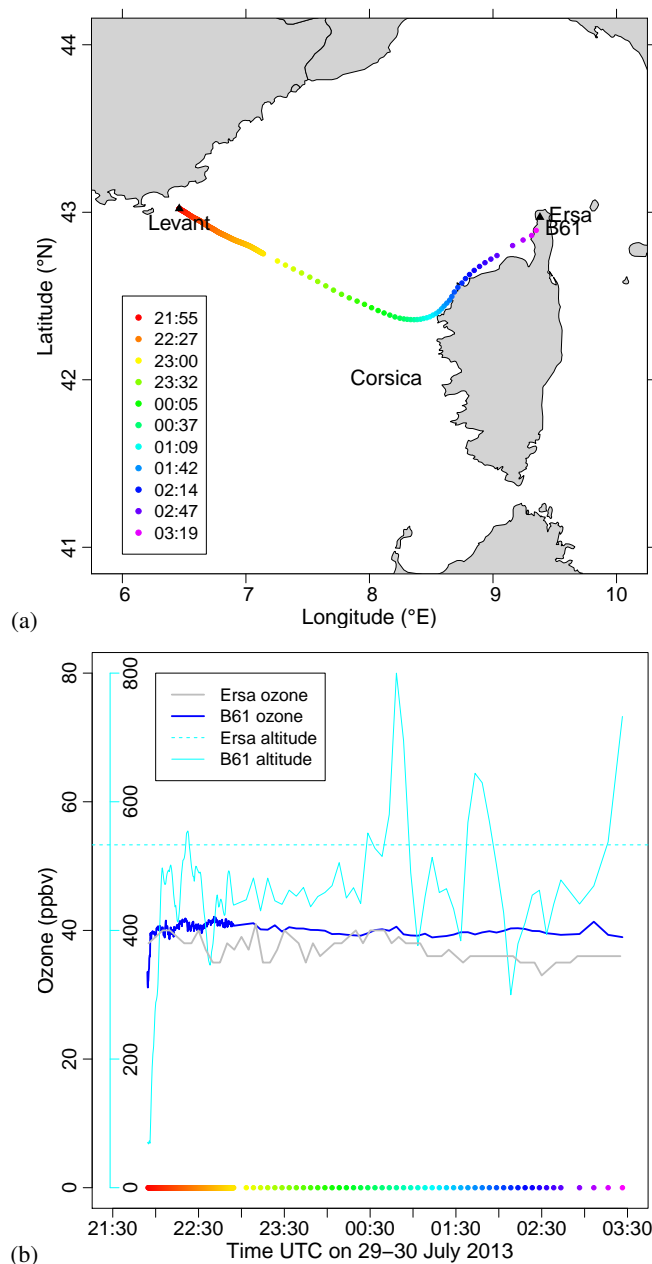
Figure 13. B61 flight on 29-30 July 2013. In both panels, the rainbow colorscale (box in panel a) represents time (UTC) at different points of the balloon trajectory. (a) B61 trajectory. (b) Ozone time series from BLPB B61 (blue curve) and Ersa surface measurements (grey curve). The cyan curve represents the balloon altitude in m asl (cyan axis). The cyan horizontal dashed line marks the altitude of the Ersa station (533 m asl). The station location is indicated in panel (a).

(a)

(b)
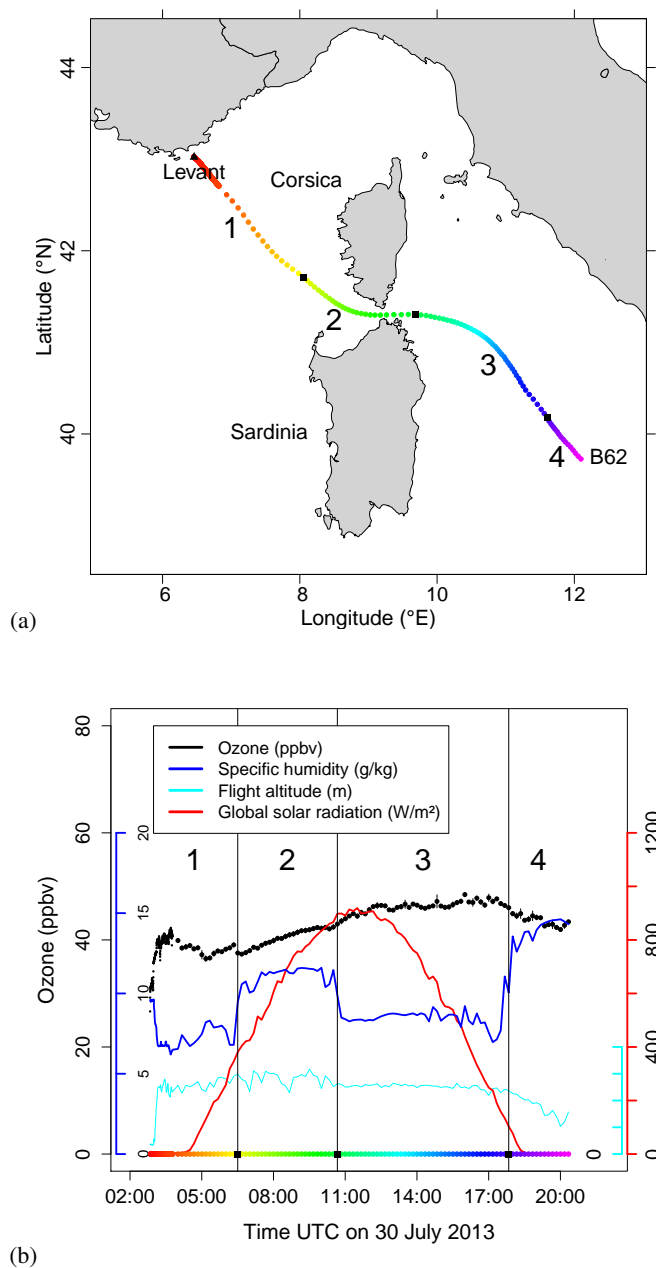
Figure 14. B62 flight launched on 30 July 2013 at 02:59 UTC. In both panels, the rainbow colorscale represents time (UTC) at different points of the balloon trajectory. Square marks delimit 4 flight sections numbered 1 to 4 (see text). (a) B62 trajectory. (b) Time-series from B62 measurements: ozone mole fraction (black dots; bars represent one standard deviation around the mean value during the measurement phase – see Sec.2.2.2); air specific humidty (blue line and related scale in g kg^{-1}); balloon flight altitude (cyan line and related scale in m asl); incoming shortwave radiation (red line and related scale in W m^{-2}).

(a)

(b)

(c)
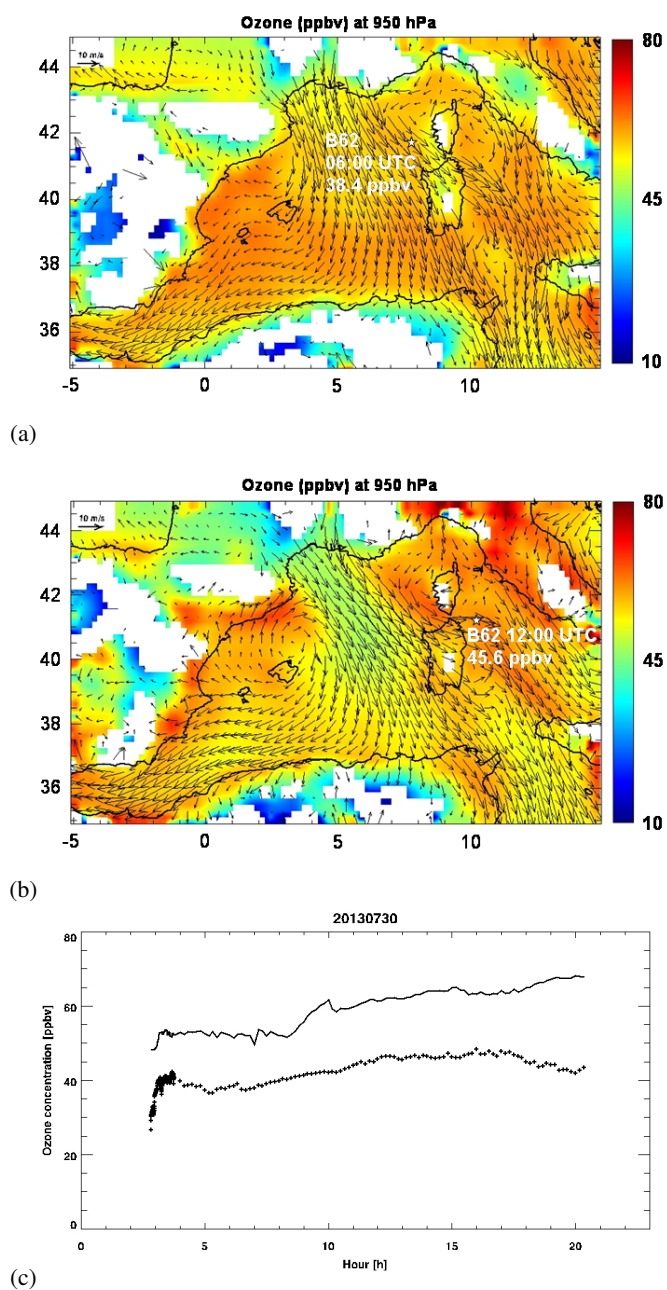
Figure 15. (a) Ozone mole fraction (color code in ppbv) and wind field (vectors) at 950 hPa pressure level given by the chemistry-transport model MOCAGE, at 06 UTC on 30 July 2013. (b) As in (a), but at 12 UTC. In panels (a) ad (b), ballon B62 positions at the respective times are marked by stars. (c) Observed (cross marks) and simulated (solid line) ozone mole fraction time series (in ppbv) recorded along the real B62 trajectory (abscissa: time UTC on 30 July 2015).
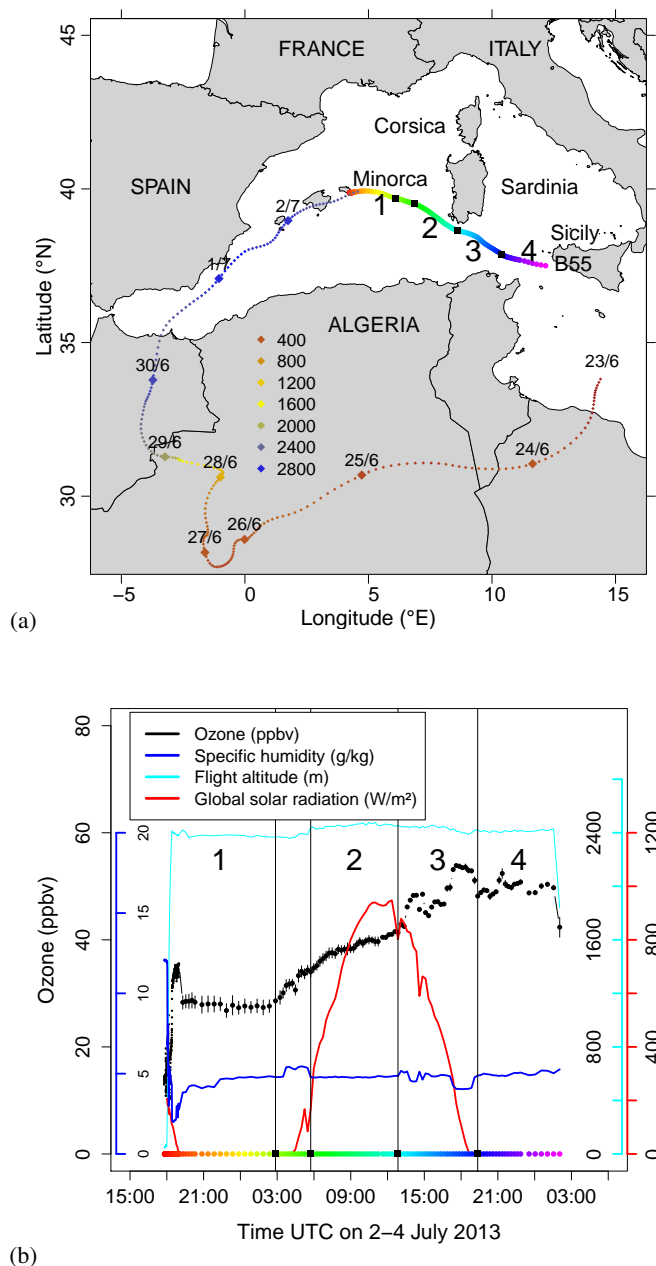
Figure 16. B55 flight launched on 2 July 2013 at 18:00 UTC. Same caption as in Fig.14 concerning the balloon. Panel (a) shows in addition a 10-day HYSPLIT backward trajectory (diamonds) ending on 2 July 2013 21:00 UTC at the current balloon position (trajectory step 1 hour; larger dots mark the parcel position daily at 00 UTC with the corresponding date; the parcel altitude represented as brown-to-blue colorscale, in m asl).